



Order and excitations in large- S kagome-lattice antiferromagnets

A. L. Chernyshev¹ and M. E. Zhitomirsky²

¹*Department of Physics and Astronomy, University of California, Irvine, California 92697, USA*

²*Service de Physique Statistique, Magnétisme et Supraconductivité, UMR-E9001 CEA-INAC/UJF, 17 rue des Martyrs, 38054 Grenoble Cedex 9, France*

(Received 26 August 2015; published 13 October 2015)

We systematically investigate the ground-state and the spectral properties of antiferromagnets on a kagomé lattice with several common types of the planar anisotropy: XXZ , single-ion, and out-of-plane Dzyaloshinskii-Moriya. Our main focus is on the role of nonlinear, anharmonic terms, which are responsible for the quantum order-by-disorder effect and for the corresponding selection of the ground-state spin structure in many of these models. The XXZ and the single-ion anisotropy models exhibit a quantum phase transition between the $\mathbf{q} = 0$ and the $\sqrt{3} \times \sqrt{3}$ states as a function of the anisotropy parameter, offering a rare example of the quantum order-by-disorder fluctuations favoring a ground state which is different from the one selected by thermal fluctuations. The nonlinear terms are also shown to be crucial for a very strong near-resonant decay phenomenon leading to the quasiparticle breakdown in the kagomé-lattice antiferromagnets whose spectra are featuring flat or weakly dispersive modes. The effect is shown to persist even in the limit of large spin values and should be common to other frustrated magnets with flat branches of excitations. Model calculations of the spectrum of the $S = 5/2$ Fe-jarosite with Dzyaloshinskii-Moriya anisotropy provide a convincing and detailed characterization of the proposed scenario.

DOI: [10.1103/PhysRevB.92.144415](https://doi.org/10.1103/PhysRevB.92.144415)

PACS number(s): 75.10.Jm, 75.30.Ds, 75.50.Ee, 78.70.Nx

I. INTRODUCTION

Kagomé-lattice antiferromagnets are iconic in the field of frustrated magnets, comprising a number of model systems whose classical ground states are massively degenerate, giving rise to an extreme sensitivity to subtle symmetry breaking effects [1,2], to fractional magnetization plateaus [3,4], to a strongly amplified role of secondary interactions [5], and to an emergent hierarchy of energy scales in their dynamics [6]. A crucial role of the nonlinear, anharmonic terms in the so-called order-by-disorder ground-state selection by thermal [7] or quantum fluctuations [8] in the kagomé-lattice antiferromagnets has been recognized for some time. Recently, an accurate, systematic treatment of the quantum order-by-disorder effect in the anisotropic versions of the model has received a significant development [9,10]. However, much less is known about the role of such terms in the excitation spectra of frustrated magnets and only recently a rather dramatic picture has begun to emerge [11].

Usually, the nonlinear terms in antiferromagnets are necessary to describe interactions of magnons and, while their role is, generally, more significant when frustration is present [12,13], they still lead to effects that are relatively minor in the large- S limit, i.e., constitute a $1/S$ contribution compared with the classical energy scale JS . However, in a wide class of highly frustrated systems, including the kagomé-lattice antiferromagnets, the nonlinear anharmonic terms are responsible for the phenomena that are much more dramatic.

First effect concerns systems in which contenders for the ground state form a highly degenerate, extensive manifold of states, and neither the classical energetics nor the harmonic fluctuations are able to select a unique ground state from that manifold [1,5,8]. In that case, the selection role is passed onto the nonlinear terms providing a variant of the quantum order by disorder effect. Such is the case of the three models considered in this work, Heisenberg, XXZ [9], and single-ion anisotropy

models, while in the case of the Dzyaloshinskii-Moriya (DM) anisotropy, a unique state is selected already on the classical level [14].

The second effect is less studied, but is equally striking. We demonstrate that the nonlinear terms lead to spectacularly strong quantum effects in the dynamical response of the flat-band frustrated magnets, even in the ones that are assumed nearly classical [11]. The resultant spectral features invoke parallels with the quasiparticle breakdown signatures in quantum spin and Bose liquids [15,16], which exhibit termination points and broad continua where single-particle excitations are no longer well-defined. In the present case, the origin of such features is in the near-resonant decay into pairs of the flat modes, facilitated by the nonlinear couplings. The effect is strongly amplified by the density of states of the flat modes and can be shown to persist even in the large- S limit, defying the usual $1/S$ suppression trend and challenging a conventional wisdom that such drastic phenomena can only occur in an inherently quantum system.

In the present study, we expand the analysis of our previous works [9,11] and offer an exposé of the $1/S$ formalism for several common anisotropic extensions of the nearest-neighbor Heisenberg model on the kagomé lattice that are also relevant to real materials. The presented approach to the nonlinear spin-wave theory can be applicable to the other, more complicated forms of the kagomé-lattice Hamiltonians as well as to a broader class of frustrated spin systems on the non-Bravais lattices. We also provide a useful extension of our approach to the perturbative treatment of small perturbations to the main Hamiltonian, such as the next-nearest superexchanges J_2 .

For the ground-state consideration, we demonstrate a quantum phase transition between the $\mathbf{q} = 0$ and the $\sqrt{3} \times \sqrt{3}$ states as a function of anisotropy parameter in two models: XXZ model, studied previously [9], and the single-ion anisotropy model. While the effect is similar in both models, the energy scale associated with it is shown to be different,

in agreement with the understanding that the degeneracy-lifting interaction is associated with high-order topologically nontrivial spin-flip processes, which are different in the two models. Nevertheless, both model cases present a rare example of the ground-state selection that is different from the choice of the thermal fluctuations, which favor the $\sqrt{3} \times \sqrt{3}$ structure for any value of the anisotropy parameter [2,5,7,9,10,17–19].

For the spectral properties of the kagomé-lattice antiferromagnets, we offer a detailed consideration of the decay-induced effects in the DM anisotropy model with J_2 , the model that closely describes the $S = 5/2$ Fe-jarosite [20,21]. We also present a general analysis of the near-resonant decays in the flat-band frustrated antiferromagnets, which suggests that the dramatic modifications in the spectrum due to this phenomenon must persist in the large- S limit. While the core of our presentation is aimed at a common and realistic extension of the nearest-neighbor Heisenberg kagomé-lattice antiferromagnet, we argue that the spectacularly strong quantum effect of the quasiparticle breakdown in an almost classical system should be applicable to a variety of other flat-band frustrated spin systems [22–25]. We also remark on a useful \mathbf{q} dependence of the dynamical structure factor, which is characteristic to the non-Bravais lattices and allows one to select spectral contributions of specific branches in the portions of the \mathbf{q} space.

The paper is organized as follows. In Sec. II we present a consideration of the harmonic theory for several common anisotropic models on the kagomé lattice, explicate details of the diagonalization procedure, and show results of a representative calculation within the harmonic approximation. In Sec. III, anharmonic terms of the models are derived and the results of the ground-state selection calculations are presented. The spectral properties of the kagomé-lattice antiferromagnets are also given a detailed exposition. Technical aspects of the derivation of the quartic terms are given in the Appendix.

II. LINEAR SPIN-WAVE THEORY

To set the stage, we provide the linear spin-wave consideration of the isotropic nearest-neighbor antiferromagnetic Heisenberg model on the kagomé lattice following the approach of Ref. [5]. We continue with various extensions of the model, which are either relevant to real materials or allow one to explore the role of quantum effects in a wider parameter space. These extensions include the anisotropic XXZ model, models with the single-ion and the out-of-plane Dzyaloshinskii-Moria anisotropies, and additional further-neighbor exchange terms. Subsequently, the important steps of the diagonalization procedure that will be essential for the nonlinear terms considered in Sec. III are exposed. In the end of this section, results of the calculations of the on-site magnetization within the linear spin-wave theory for the XXZ model are presented as an example.

A. Nearest-neighbor Heisenberg model

Within the spin-wave treatment, nearest-neighbor Heisenberg antiferromagnet on the kagomé lattice with the Hamiltonian

$$\hat{H} = J \sum_{\langle ij \rangle} \mathbf{S}_i \cdot \mathbf{S}_j \quad (1)$$

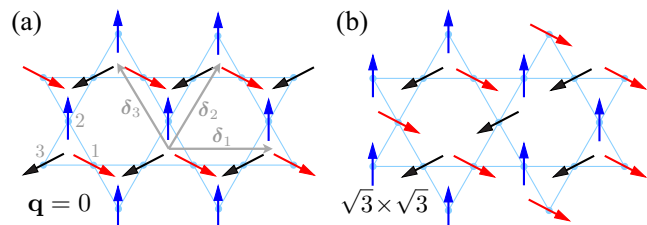


FIG. 1. (Color online) (a) $\mathbf{q} = 0$ and (b) $\sqrt{3} \times \sqrt{3}$ spin configurations. In (a), primitive vectors of the kagomé lattice and numbering of sites within the unit cell are shown.

is assumed to be in an ordered state with spins forming a coplanar 120° structure. Summation is over bonds and i, j are the sites of the lattice. Aligning the z axis on each site along the direction of the ordered moment and directing the y axes out of the ordering plane transforms the Hamiltonian (1) to a local spin basis

$$\begin{aligned} \hat{H} &= J \sum_{\langle ij \rangle} (S_i^y S_j^y + \cos \theta_{ij} (S_i^x S_j^x + S_i^z S_j^z)) \\ &\quad + \sin \theta_{ij} (S_i^z S_j^x - S_i^x S_j^z) \\ &= J \sum_{\langle ij \rangle} \mathbf{S}_i \otimes \mathbf{S}_j, \end{aligned} \quad (2)$$

where $\theta_{ij} = \theta_i - \theta_j$ is an angle between two neighboring spins and we have introduced “matrix” product \otimes of spins with the matrix

$$\otimes = \begin{pmatrix} \cos \theta_{ij} & 0 & -\sin \theta_{ij} \\ 0 & 1 & 0 \\ \sin \theta_{ij} & 0 & \cos \theta_{ij} \end{pmatrix} \quad (3)$$

as a shorthand notation.

We choose the unit cell of the kagomé lattice as an up-triangle, see Fig. 1, and the primitive vectors of the corresponding triangular Bravais lattice as

$$\delta_1 = (1, 0), \quad \delta_2 = \left(\frac{1}{2}, \frac{\sqrt{3}}{2} \right), \quad \delta_3 = \delta_2 - \delta_1, \quad (4)$$

all in units of $2a$ where a is the interatomic distance. The atomic coordinates within the unit cell are $\rho_1 = 0$, $\rho_2 = \frac{1}{2}\delta_3$, and $\rho_3 = -\frac{1}{2}\delta_1$.

Then, changing summation over bonds to summation over unit cells and the atomic index, $i \rightarrow \{\alpha, \ell\}$, with $\alpha = 1 - 3$ enumerating atoms within the unit cell, the Hamiltonian (2) becomes

$$\begin{aligned} \hat{H} &= J \sum_{\ell} \mathbf{S}_{1,\ell} \otimes (\mathbf{S}_{2,\ell} + \mathbf{S}_{2,\ell-3}) \\ &\quad + \mathbf{S}_{1,\ell} \otimes (\mathbf{S}_{3,\ell} + \mathbf{S}_{3,\ell+1}) + \mathbf{S}_{2,\ell} \otimes (\mathbf{S}_{3,\ell} + \mathbf{S}_{3,\ell+2}), \end{aligned} \quad (5)$$

where the product $\mathbf{S}_{\alpha,\ell} \otimes \mathbf{S}_{\alpha',\ell'}$ is according to (2), and $\ell \pm n \equiv \mathbf{R}_{\ell} \pm \delta_n$ with the coordinate of the unit cell $\mathbf{R}_{\ell} = m_1 \delta_1 + m_2 \delta_2$.

B. Harmonic spin-wave approximation

It should be noted that although a coplanar state with spins on each triangle in a 120° structure minimizes the classical

energy of (1), such a state is not unique and the manifold of them is extensive [26]. However, it is also clear from the Hamiltonian in the local basis (2) that the linear spin-wave theory is the same for *any* state from this degenerate manifold [1], because $\cos \theta_{ij} = -1/2$ for any pair of spins in such state and $S^x S^z$ terms do not contribute to the harmonic order of the $1/S$ expansion.

Thus we introduce Holstein-Primakoff representation for spin operators

$$S_{\alpha,\ell}^z = S - a_{\alpha,\ell}^\dagger a_{\alpha,\ell}, \quad S_{\alpha,\ell}^- = a_{\alpha,\ell}^\dagger \sqrt{2S - a_{\alpha,\ell}^\dagger a_{\alpha,\ell}} \quad (6)$$

into (5) and, keeping only quadratic terms, obtain a harmonic Hamiltonian for three species of bosons

$$\begin{aligned} \hat{\mathcal{H}}_2 = 2JS \sum_{\ell} & \left\{ [a_{1,\ell}^\dagger a_{1,\ell} + a_{2,\ell}^\dagger a_{2,\ell} + a_{3,\ell}^\dagger a_{3,\ell}] \right. \\ & + \frac{1}{8} [a_{1,\ell}^\dagger (a_{2,\ell} + a_{2,\ell-3}) + a_{1,\ell}^\dagger (a_{3,\ell} + a_{3,\ell+1}) \\ & + a_{2,\ell}^\dagger (a_{3,\ell} + a_{3,\ell+2}) + \text{H.c.}] \\ & - \frac{3}{8} [a_{1,\ell} (a_{2,\ell} + a_{2,\ell-3}) + a_{1,\ell} (a_{3,\ell} + a_{3,\ell+1}) \\ & \left. + a_{2,\ell} (a_{3,\ell} + a_{3,\ell+2}) + \text{H.c.}] \right\}. \quad (7) \end{aligned}$$

Performing the Fourier transformation according to

$$a_{\alpha,\ell} = \frac{1}{\sqrt{N}} \sum_{\mathbf{k}} a_{\alpha,\mathbf{k}} e^{i\mathbf{k}\mathbf{r}_{\alpha,\ell}}, \quad (8)$$

where $\mathbf{r}_{\alpha,\ell} = \mathbf{R}_\ell + \boldsymbol{\rho}_\alpha$ and N is the number of unit cells, we obtain the linear spin-wave theory Hamiltonian

$$\begin{aligned} \hat{\mathcal{H}}_2 = 2JS \sum_{\mathbf{k},\alpha\beta} & \left\{ \left[\delta_{\alpha\beta} + \frac{1}{4} \Lambda_{\mathbf{k}}^{\alpha\beta} \right] a_{\alpha,\mathbf{k}}^\dagger a_{\beta,\mathbf{k}} \right. \\ & \left. - \frac{3}{8} \Lambda_{\mathbf{k}}^{\alpha\beta} (a_{\alpha,\mathbf{k}}^\dagger a_{\beta,-\mathbf{k}}^\dagger + \text{H.c.}) \right\}, \quad (9) \end{aligned}$$

with the matrix

$$\hat{\Lambda}_{\mathbf{k}} = \begin{pmatrix} 0 & c_3 & c_1 \\ c_3 & 0 & c_2 \\ c_1 & c_2 & 0 \end{pmatrix}, \quad (10)$$

and shorthand notations $c_n = \cos(q_n)$ with $q_n = \mathbf{k} \cdot \boldsymbol{\delta}_n/2$.

One can rewrite this Hamiltonian as

$$\hat{\mathcal{H}}_2 = \sum_{\mathbf{k}>0} \hat{X}_{\mathbf{k}}^\dagger \hat{\mathbf{H}}_{\mathbf{k}} \hat{X}_{\mathbf{k}} - 3JS, \quad (11)$$

with the vector operator

$$\hat{X}_{\mathbf{k}}^\dagger = (a_{1,\mathbf{k}}^\dagger, a_{2,\mathbf{k}}^\dagger, a_{3,\mathbf{k}}^\dagger, a_{1,-\mathbf{k}}, a_{2,-\mathbf{k}}, a_{3,-\mathbf{k}}) \quad (12)$$

and the 6×6 matrix $\hat{\mathbf{H}}_{\mathbf{k}}$

$$\hat{\mathbf{H}}_{\mathbf{k}} = 2JS \begin{pmatrix} \hat{\Lambda}_{\mathbf{k}} & -\hat{\mathbf{B}}_{\mathbf{k}} \\ -\hat{\mathbf{B}}_{\mathbf{k}} & \hat{\Lambda}_{\mathbf{k}} \end{pmatrix}, \quad (13)$$

where

$$\hat{\Lambda}_{\mathbf{k}} = \hat{\mathbf{I}} + \frac{1}{4} \hat{\Lambda}_{\mathbf{k}}, \quad \hat{\mathbf{B}}_{\mathbf{k}} = \frac{3}{4} \hat{\Lambda}_{\mathbf{k}}, \quad (14)$$

and $\hat{\mathbf{I}}$ is the identity matrix.

For a moment, we will confine ourselves to the eigenvalue problem of $\hat{\mathcal{H}}_2$. Because of an obvious commutativity of the matrices $\hat{\Lambda}_{\mathbf{k}}$ and $\hat{\mathbf{B}}_{\mathbf{k}}$, the eigenvalues of $\hat{\mathbf{H}}_{\mathbf{k}}$ are straightforwardly related to their eigenvalues, and, in turn, are determined by the eigenvalues $\lambda_{\nu,\mathbf{k}}$ of the matrix $\hat{\Lambda}_{\mathbf{k}}$, so that the spin-wave excitation energies are

$$\varepsilon_{\nu,\mathbf{k}} = 2JS \sqrt{A_{\nu,\mathbf{k}}^2 - B_{\nu,\mathbf{k}}^2} = 2JS \omega_{\nu,\mathbf{k}}, \quad (15)$$

with the frequencies $\omega_{\nu,\mathbf{k}} = \sqrt{(1 - \lambda_{\nu,\mathbf{k}}/2)(1 + \lambda_{\nu,\mathbf{k}})}$ and

$$A_{\nu,\mathbf{k}} = 1 + \frac{1}{4} \lambda_{\nu,\mathbf{k}}, \quad B_{\nu,\mathbf{k}} = \frac{3}{4} \lambda_{\nu,\mathbf{k}}. \quad (16)$$

Thus the problem of the diagonalization of $\hat{\mathcal{H}}_2$ in (9) is reduced to the eigenvalue problem of $\hat{\Lambda}_{\mathbf{k}}$ in (10). From the characteristic equation for $\hat{\Lambda}_{\mathbf{k}}$ one finds

$$|\hat{\Lambda}_{\mathbf{k}} - \lambda| = (\lambda + 1)(\lambda^2 - \lambda - 2\gamma_{\mathbf{k}}) = 0, \quad (17)$$

where $\gamma_{\mathbf{k}} \equiv c_1 c_2 c_3$ is introduced and factorization is performed with the help of a useful identity

$$c_1^2 + c_2^2 + c_3^2 = 1 + 2c_1 c_2 c_3,$$

which holds once the cosine arguments satisfy $q_2 = q_1 + q_3$. Thus the $\lambda_{\nu,\mathbf{k}}$ eigenvalues are

$$\lambda_1 = -1, \quad \lambda_{2(3),\mathbf{k}} = \frac{1}{2}(1 \pm \sqrt{1 + 8\gamma_{\mathbf{k}}}). \quad (18)$$

Of the resultant spin-wave excitations one is completely dispersionless and has zero energy, referred to as the ‘‘flat mode,’’ and two are ‘‘normal,’’ i.e., dispersive modes, which are degenerate in the Heisenberg limit

$$\varepsilon_{1,\mathbf{k}} = 0, \quad \varepsilon_{2(3),\mathbf{k}} = 2JS \sqrt{1 - \gamma_{\mathbf{k}}}. \quad (19)$$

The nature of the flat mode has been discussed previously [1,5,8]. Generally, such modes owe their origin to both the topological structure of the underlying lattices that facilitate spin frustration and the insufficient constraint on the manifold of spin configurations. Physically, they correspond to the localized, alternating out-of-plane fluctuations of spins around elementary hexagons [1,5], which do not experience a restoring force in the harmonic order in the Heisenberg limit; hence their energy is zero. In the following, various anisotropies lift the energy of such a flat mode, but preserve its flatness.

C. XXZ model

Next, we consider an extension of the Heisenberg model on the kagomé lattice to the XXZ model with anisotropy of the easy-plane type, $0 \leq \Delta \leq 1$. The original motivation for this extension, see Ref. [9], was that the degeneracy among the 120° coplanar states in this model remains the same as in the Heisenberg model. This has allowed us to extend the parameter space and to study the effect of quantum fluctuations in the ground-state selection without lifting degeneracy of the classical ground-state manifold; see Sec. III for more detail [9].

In the case of the XXZ model, the plane for the coplanar 120° structure is chosen by the anisotropy. In the local spin basis of (2) with y axis out of the ordering plane, the XXZ

addition to the Heisenberg model reads as

$$\delta\hat{\mathcal{H}} = J(\Delta - 1) \sum_{\langle ij \rangle} S_i^y S_j^y. \quad (20)$$

A now straightforward spin-wave algebra of (20) leaves the structure of the harmonic Hamiltonian in (9) intact, yielding corrections to the Hamiltonian matrix in (13)

$$\delta\hat{\mathbf{A}}_{\mathbf{k}} = \delta\hat{\mathbf{B}}_{\mathbf{k}} = \frac{(\Delta - 1)}{2} \hat{\mathbf{A}}_{\mathbf{k}}. \quad (21)$$

The spin-wave energies for the XXZ model in (15) are now with $\omega_{v,\mathbf{k}} = \sqrt{(1 - \lambda_{v,\mathbf{k}}/2)(1 + \Delta\lambda_{v,\mathbf{k}})}$ and give

$$\varepsilon_{1,\mathbf{k}} = 2JS\sqrt{3(1 - \Delta)/2}, \quad (22)$$

for the flat mode, which is now at a finite energy, and

$$\varepsilon_{2(3),\mathbf{k}} = 2JS\sqrt{1 - \Delta\gamma_{\mathbf{k}} - (1 - \Delta)(1 \pm \sqrt{1 + 8\gamma_{\mathbf{k}}})/4}$$

for the dispersive modes.

D. Single-ion anisotropy

Instead of the XXZ correction (20), an alternative way of generating easy-plane anisotropy is to add a positive single-ion term

$$\delta\hat{\mathcal{H}} = D \sum_i (S_i^y)^2, \quad (23)$$

where y is the out-of-plane axis in the local spin basis of (2) as before. This term, in a complete similarity to the XXZ case, gives zero contribution to the classical energy, does not affect cubic anharmonicity, and does not contribute to the degeneracy lifting of the 120° manifold through the quartic terms [9]. Its contribution to the harmonic Hamiltonian (13) is also simple

$$\delta\hat{\mathbf{A}}_{\mathbf{k}} = \delta\hat{\mathbf{B}}_{\mathbf{k}} = \frac{d}{2} \hat{\mathbf{I}}, \quad (24)$$

where $d = D/J$ and $\hat{\mathbf{I}}$ is the identity matrix. Thus, once again, the eigenvalue problem of $\hat{\mathcal{H}}_2$ reduces to the eigenvalue problem of $\hat{\mathbf{A}}_{\mathbf{k}}$, resulting in the spin-wave frequencies $\omega_{v,\mathbf{k}} = \sqrt{(1 - \lambda_{v,\mathbf{k}}/2)(1 + d + \lambda_{v,\mathbf{k}})}$, and the spin-wave energy of the flat mode

$$\varepsilon_{1,\mathbf{k}} = 2JS\sqrt{3d/2}, \quad (25)$$

while energies of the dispersive modes are

$$\varepsilon_{2(3),\mathbf{k}} = 2JS\sqrt{1 + d - \gamma_{\mathbf{k}} - d(1 \pm \sqrt{1 + 8\gamma_{\mathbf{k}}})/4}, \quad (26)$$

which should be compared to the XXZ results above.

There is a high degree of similarity of the single-ion anisotropy model (23) and its results to the XXZ case, the most important being no degeneracy lifting among the 120° manifold of classical states at the harmonic level of approximation. However, there is also an important difference. If analyzed in real space in the local basis (2), the structure of the spin-flip terms is different in the two models. In particular, the single-ion term (23) creates spin flips that are purely local, while the spin-flip hopping and other amplitudes responsible for degeneracy lifting remain independent of anisotropy D . Therefore, from the point of view of the real-space perturbation theory, described in Ref. [9], the minimal order in which an

effective degeneracy-lifting interaction is generated is different in the two models [27]. We will address this difference in Sec. III in more detail.

E. Dzyaloshinskii-Moria interaction

An important correction to the Heisenberg spin model (1) that commonly occurs in real magnetic materials with the kagomé structure is the anisotropic Dzyaloshinskii-Moriya (DM) interaction.

The out-of-plane DM term, see Fig. 2, is the main perturbation to the Heisenberg Hamiltonian of the $S = 5/2$ kagomé-lattice antiferromagnet Fe-jarosite [20,21], $S = 1/2$ materials herbertsmithite [28] and vesignieite [29], and other systems [30]. This anisotropy differs from the ones considered above in a number of aspects, but allows for a very similar analytical treatment, mainly because of its nearest-neighbor nature.

The antisymmetric Dzyaloshinskii-Moriya interaction is generally written as

$$\delta\hat{\mathcal{H}}_{DM} = \sum_{\langle ij \rangle} \mathbf{D}_{ij} \cdot (\mathbf{S}_i \times \mathbf{S}_j). \quad (27)$$

In order to determine the DM vectors \mathbf{D}_{ij} one has to specify the order of sites in the vector product, which may be represented by the bond direction from the first to the second spin in each pair. A convenient choice consists of ordering spins uniformly along the chains; see Fig. 2. Then, the symmetry analysis yields a unique pattern of the DM vectors orthogonal to the kagomé plane as shown in Fig. 2 [14,31,32]. Note that the in-plane components of the DM vectors are strictly forbidden once the kagomé plane coincides with a mirror crystal plane [31].

Apparent alternation of the DM vectors between up triangles with $\mathbf{D}_{ij} = (0,0,-D_z)$ and down triangles with $\mathbf{D}_{ij} = (0,0,D_z)$ is partly fictitious, because it is a consequence of the chosen bond gauge, in which the two types of triangles are circumvented oppositely; see Fig. 2. The DM interactions on the two triangles favor the same sense of spin rotation or chirality. Hence, for a given sign of D_z , the DM term

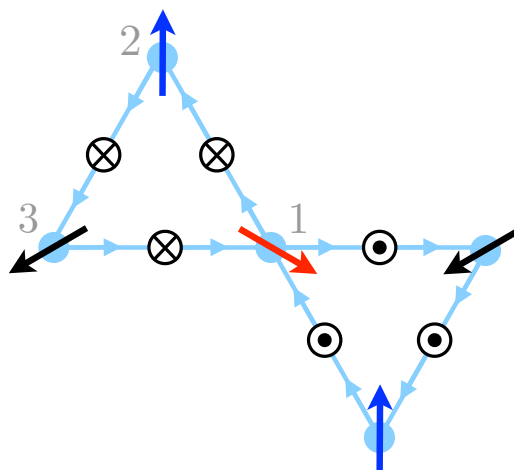


FIG. 2. (Color online) Directions of the out-of-plane DM vectors. Arrows on the bonds show the ordering of the \mathbf{S}_i and \mathbf{S}_j operators in the vector product in (27).

(27) selects one of the two $\mathbf{q} = 0$ structures with positive ($D_z > 0$) or negative ($D_z < 0$) chiralities, yielding energy gain $E_{\text{cl}} = -\sqrt{3}|D_z|S^2$ per site. On the other hand, for the $\sqrt{3} \times \sqrt{3}$ state contributions from up and down triangles come with opposite sign and cancel out. In the following, we assume $D_z > 0$ and, consequently, perform the spin-wave expansion around the $\mathbf{q} = 0$ state with positive chiralities; see Fig. 2. It is also straightforward to see that the DM term does not induce additional canting and preserves the 120° magnetic structure in the x - y plane.

Consider the DM term (27) on the (1,2) bond in Fig. 2 written in the rotating local spin basis (2)

$$\begin{aligned} \hat{\mathcal{H}}^{(1,2)} = & D_z \sin \theta_{12} (S_2^z S_1^z + S_2^x S_1^x) \\ & + D_z \cos \theta_{12} (S_2^z S_1^x - S_2^x S_1^z), \end{aligned} \quad (28)$$

where $\theta_{ij} = \theta_i - \theta_j$, and the first term contributes to the classical, harmonic, and quartic orders of the $1/S$ expansion, while the second contributes in the cubic order.

Since the DM term concerns only the nearest-neighbor pairs of spins and because in the $\mathbf{q} = 0$ state all DM bonds contribute identically, the overall structure of the harmonic part of the Hamiltonian remains the same as in (9). Then, some algebra yields the harmonic Hamiltonian $\hat{\mathcal{H}}_2$ in the form (13) with the DM contributions

$$\delta \hat{\mathbf{A}}_{\mathbf{k}} = d_M \left(\hat{\mathbf{I}} - \frac{1}{4} \hat{\mathbf{A}}_{\mathbf{k}} \right), \quad \delta \hat{\mathbf{B}}_{\mathbf{k}} = \frac{d_M}{4} \hat{\mathbf{A}}_{\mathbf{k}}, \quad (29)$$

where $d_M = \sqrt{3}D_z/J$ and $\hat{\mathbf{A}}_{\mathbf{k}}$ is unchanged from (10), again reducing the eigenvalue problem of the harmonic spin-wave theory to the one of $\hat{\mathbf{A}}_{\mathbf{k}}$, already solved in (17) and (18). Then, the spin-wave frequencies for the problem with the out-of-plane DM interaction (27) are $\omega_{\nu, \mathbf{k}} = \sqrt{(1 + d_M)(1 - \lambda_{\nu, \mathbf{k}}/2)(1 + d_M + \lambda_{\nu, \mathbf{k}})}$. With $\lambda_{\nu, \mathbf{k}}$ from (18), the flat mode energy is

$$\varepsilon_{1, \mathbf{k}} = 2JS\sqrt{3d_M(1 + d_M)/2}, \quad (30)$$

and the energies of the dispersive modes are

$$\begin{aligned} \varepsilon_{2(3), \mathbf{k}} = & 2JS\sqrt{1 + d_M} \\ & \times \sqrt{1 + d_M - \gamma_{\mathbf{k}} - d_M(1 \pm \sqrt{1 + 8\gamma_{\mathbf{k}}})/4}, \end{aligned} \quad (31)$$

which are similar to the XXZ (22) and the single-ion (25), (26) results and are in agreement with Ref. [21]. The energies of the magnon modes $\varepsilon_{\nu, \mathbf{k}}$ are illustrated in Fig. 3 for the DM term $D_z/J = 0.06$, a value relevant to the Fe-jarosite [20,21].

Opposite to the previous extensions, the DM term contributes to the cubic anharmonicities; see (28). Using the second term in (28) for one bond and extending it to the entire lattice we find for the $\mathbf{q} = 0$ state

$$\hat{\mathcal{H}}_3 = \frac{d_M}{3} J \sqrt{\frac{S}{2}} \sum_{i,j} \sin \theta_{ij} (a_i^\dagger a_j^\dagger a_j + \text{H.c.}), \quad (32)$$

whose structure is identical to the cubic term from the J part of the Hamiltonian (47) considered in Sec. III. Thus the out-of-plane DM interaction in the $\mathbf{q} = 0$ state simply renormalizes cubic vertices by a factor $(1 + d_M/3)$.

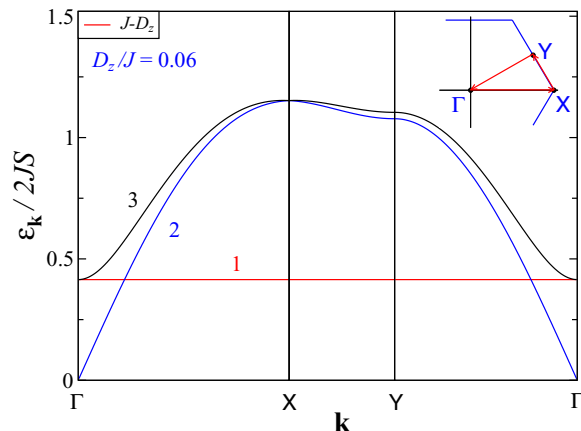


FIG. 3. (Color online) Energies of the three magnon modes for the J - D_z spin model with the out-of-plane DM interaction $D_z/J = 0.06$ along a representative path in the Brillouin zone.

F. Small- J_2 expansion

In the Heisenberg kagomé-lattice antiferromagnet, additional next-nearest-neighbor coupling J_2 lifts the degeneracy of the 120° manifold of classical states and selects between the $\mathbf{q} = 0$ and $\sqrt{3} \times \sqrt{3}$ ground states [5,8]. It also introduces a dispersion into the “flat mode” energy and thus was invoked to reproduce experimentally observed \mathbf{k} dependence of such mode in Fe-jarosite [21]. We note, however, that quantum fluctuations beyond the harmonic order also generate effective J_2 interactions [8,9], and thus could be the source of the same \mathbf{k} dependence. As we show in Sec. III, the dispersion of the flat mode is particularly important for the quasiresonant spin-wave decays. Below, we consider the effect of small J_2 perturbatively. Other types of small interactions can be taken into account in a similar fashion.

We first point out that the network of the second-neighbor bonds forms three independent kagomé lattices. Second, these bonds connect only spins from different sublattices of the original lattice; see Fig. 1. Therefore, contribution of the J_2 term to the harmonic spin-wave Hamiltonian has the same structure as the nearest-neighbor Hamiltonian (9)

$$\begin{aligned} \delta \hat{\mathcal{H}}'_2 = & 2J_2 S \sum_{\mathbf{k}, \alpha\beta} \left\{ \left[\delta_{\alpha\beta} + \frac{1}{4} \Lambda_{\mathbf{k}}^{\prime\alpha\beta} \right] a_{\alpha, \mathbf{k}}^\dagger a_{\beta, \mathbf{k}} \right. \\ & \left. - \frac{3}{8} \Lambda_{\mathbf{k}}^{\prime\alpha\beta} (a_{\alpha, \mathbf{k}}^\dagger a_{\beta, -\mathbf{k}}^\dagger + \text{H.c.}) \right\}, \end{aligned} \quad (33)$$

where instead of $\hat{\mathbf{A}}_{\mathbf{k}}$ the matrix is

$$\hat{\mathbf{A}}'_{\mathbf{k}} = \begin{pmatrix} 0 & c'_3 & c'_1 \\ c'_3 & 0 & c'_2 \\ c'_1 & c'_2 & 0 \end{pmatrix}, \quad (34)$$

and we use the shorthand notations $c'_1 = \cos(q_3 + q_2)$, $c'_2 = \cos(q_3 - q_1)$, $c'_3 = \cos(q_1 + q_2)$, with $q_n = \mathbf{k} \cdot \boldsymbol{\delta}_n/2$.

Therefore, the diagonalization of the harmonic part of the $J - J_2$ Hamiltonian requires diagonalization of the matrix $\tilde{\mathbf{A}}_{\mathbf{k}} = \hat{\mathbf{A}}_{\mathbf{k}} + j_2 \hat{\mathbf{A}}'_{\mathbf{k}}$, where $j_2 = J_2/J$. Generally, this can be done numerically, the approach taken in Ref. [21] in the analysis of the Fe-jarosite spectrum, with the analytical results

given only for the high-symmetry points. However, having in mind the problem of spin-wave excitation in large- S kagomé-lattice antiferromagnet, for the physical range of interest $J_2 \ll J$ one can make analytical progress using an expansion in j_2 .

Because the most important qualitative effect of J_2 is the dispersion of the flat band, we will ignore small corrections to the “normal” modes. Expanding the characteristic equation for the matrix $\tilde{\Lambda}_{\mathbf{k}}$ in j_2 we obtain

$$\begin{aligned}
(\lambda + 1)(\lambda^2 - \lambda - 2\gamma_{\mathbf{k}}) &= 2j_2(\lambda f_1(\mathbf{k}) + f_2(\mathbf{k})), \\
\text{where } f_1(\mathbf{k}) &= c'_1 c_1 + c'_2 c_2 + c'_3 c_3, \\
f_2(\mathbf{k}) &= c'_1 c_2 c_3 + c'_2 c_1 c_3 + c'_3 c_1 c_2. \quad (35)
\end{aligned}$$

Then, the flat mode $\lambda_1 = -1$ eigenvalue is modified as

$$\tilde{\lambda}_{1,\mathbf{k}} = \lambda_1 + j_2 \lambda_{1,\mathbf{k}}^{(1)}, \quad \lambda_{1,\mathbf{k}}^{(1)} = \left(\frac{f_2(\mathbf{k}) - f_1(\mathbf{k})}{1 - \gamma_{\mathbf{k}}} \right). \quad (36)$$

Corrections to λ_2 and λ_3 can be obtained similarly.

Having this perturbative correction to λ_1 in (36) allows us to obtain the flat mode energies in various models. We list some of the answers below.

(i) $J - J_2$ Heisenberg model:

$$\varepsilon_{1,\mathbf{k}} = 2JS\sqrt{3j_2(1 + \lambda_{1,\mathbf{k}}^{(1)})/2} + O(j_2^{3/2}). \quad (37)$$

(ii) $J - J_2$ XXZ model. Here we assume that the anisotropy Δ is the same in both exchanges:

$$\begin{aligned}
\varepsilon_{1,\mathbf{k}} &= 2JS\sqrt{3/2 + j_2(1 - \lambda_{1,\mathbf{k}}^{(1)})} \\
&\times \sqrt{1 - \Delta + j_2(1 + \lambda_{1,\mathbf{k}}^{(1)})} + O(j_2^2). \quad (38)
\end{aligned}$$

(iii) $J - J_2$ out-of-plane DM model.

$$\begin{aligned}
\varepsilon_{1,\mathbf{k}} &= 2JS\sqrt{3(1 + d_M)/2 + j_2(1 - \lambda_{1,\mathbf{k}}^{(1)})} \\
&\times \sqrt{d_M + j_2(1 + \lambda_{1,\mathbf{k}}^{(1)})} + O(j_2^2), \quad (39)
\end{aligned}$$

where $d_M = \sqrt{3}D_z/J$ as before. This is the model which was used to describe the spectrum of Fe-jarosite [21]. Our results agree exactly with the expressions for the high-symmetry points provided in Ref. [21]. The advantage of our approach is that it is fully analytical in the entire Brillouin zone.

Effects of the second-neighbor exchange J_2 and the DM coupling D_z on the dispersion of the flat mode $\varepsilon_{1,\mathbf{k}}$ are summarized in Fig. 4 for representative values $J_2/J = 0.03$ and $D_z/J = 0.06$ that are motivated by the experimental data for Fe-jarosite [20,21]; the $J_2 = 0$ energies are also shown. In the same figure the energies obtained via numerical diagonalization of the matrix $\tilde{\Lambda}_{\mathbf{k}}$ are shown. The corresponding results are indistinguishable from the approximate results of Eqs. (37) and (39) on the scale of our plot.

G. Two-step diagonalization

For the above three cases, the XXZ , the single-ion, and the out-of-plane DM models, the harmonic spin-wave theory includes diagonalization of the same matrix $\hat{\Lambda}_{\mathbf{k}}$. Here we elaborate on details of this general procedure and provide the

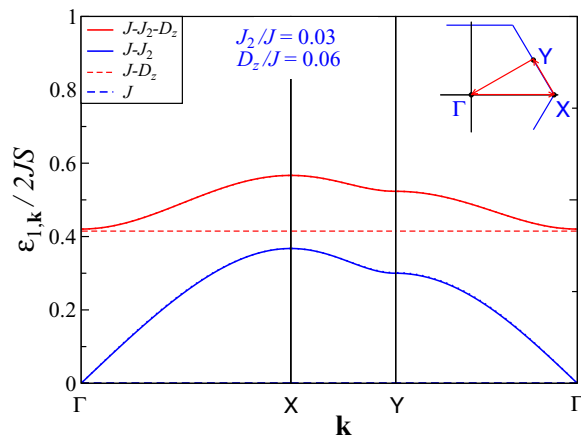


FIG. 4. (Color online) Evolution of the “flat mode” upon switching on additional interactions with parameters shown in the legend. Solid lines: energies of the flat mode for the $J - J_2$ Heisenberg (lower curve) and out-of-plane DM models (upper curve), using approximate expressions in Eqs. (37) and (39). Dashed lines are the energies for the same models at $J_2 = 0$. Dotted lines (virtually indistinguishable from solid lines) are exact results, without using the expansion in J_2 .

formalism, which is essential for treating the nonlinear terms in all these models and is identical for all considered cases.

Following Ref. [5], diagonalization of $\hat{\Lambda}_{\mathbf{k}}$ implies a two-step diagonalization procedure of $\hat{\mathcal{H}}_2$ in the form (13). Its eigenvectors $\mathbf{w}_v^\dagger = (w_{v,1}(\mathbf{k}), w_{v,2}(\mathbf{k}), w_{v,3}(\mathbf{k}))$ obey

$$\hat{\Lambda}_{\mathbf{k}} \mathbf{w}_v = \lambda_{v,\mathbf{k}} \mathbf{w}_v \quad (40)$$

and can be found explicitly [5,9]

$$\mathbf{w}_v(\mathbf{k}) = \frac{1}{r_v} \begin{pmatrix} c_1 c_2 + \lambda_v c_3 \\ \lambda_v^2 - c_1^2 \\ c_1 c_3 + \lambda_v c_2 \end{pmatrix}, \quad (41)$$

with $r_v = \sqrt{(c_1 c_2 + \lambda_v c_3)^2 + (\lambda_v^2 - c_1^2)^2 + (c_1 c_3 + \lambda_v c_2)^2}$.

These eigenvectors define a unitary transformation of the original Holstein-Primakoff bosons to the new ones

$$a_{\alpha,\mathbf{k}} = \sum_v w_{v,\alpha}(\mathbf{k}) d_{v,\mathbf{k}}, \quad d_{v,\mathbf{k}} = \sum_\alpha w_{v,\alpha}(\mathbf{k}) a_{\alpha,\mathbf{k}}, \quad (42)$$

such that the harmonic Hamiltonian $\hat{\mathcal{H}}_2$ in the form of (9) with $\hat{\mathbf{A}}_{\mathbf{k}}$'s and $\hat{\mathbf{B}}_{\mathbf{k}}$'s from (14) with (21), (24), or (29) is turned into three independent Hamiltonians

$$\hat{\mathcal{H}}_2 = 2JS \sum_{v,\mathbf{k}} \left[A_{v,\mathbf{k}} d_{v,\mathbf{k}}^\dagger d_{v,\mathbf{k}} - \frac{B_{v,\mathbf{k}}}{2} (d_{v,\mathbf{k}}^\dagger d_{v,-\mathbf{k}}^\dagger + \text{H.c.}) \right].$$

The final step is the conventional Bogolyubov transformation for each individual species of the d bosons

$$d_{v,\mathbf{k}} = u_{v\mathbf{k}} b_{v,\mathbf{k}} + v_{v\mathbf{k}} b_{v,-\mathbf{k}}^\dagger, \quad (43)$$

with $u_{v\mathbf{k}}^2 - v_{v\mathbf{k}}^2 = 1$ and

$$v_{v\mathbf{k}}^2 = \frac{1}{2} \left(\frac{A_{v,\mathbf{k}}}{\omega_{v,\mathbf{k}}} - 1 \right), \quad 2u_{v\mathbf{k}} v_{v\mathbf{k}} = \frac{B_{v,\mathbf{k}}}{\omega_{v,\mathbf{k}}}, \quad (44)$$

where the eigenvalues $\omega_{v,\mathbf{k}}$, $A_{v,\mathbf{k}}$, and $B_{v,\mathbf{k}}$ were obtained for each of the models in previous sections. The importance of

this two-step procedure will be apparent in the discussions of the nonlinear terms in Sec. III.

H. Ordered magnetic moment

Here we discuss the dependence of the ordered magnetic moment on anisotropy parameter and on the value of the spin S . While we only consider the XXZ model [9], the results are expected to be similar for the other anisotropies considered above. It should be noted that this calculation can only qualitatively estimate the stability of the Néel order, because it only includes the “diagonal” quantum fluctuation for a given state, completely neglecting the “off-diagonal” tunneling processes between different states within the manifold. On the other hand, such processes should be exponentially suppressed for larger spins [33].

Within the linear spin-wave theory, magnetic moment on a site that belongs to the sublattice α is reduced by zero-point fluctuations: $\langle S \rangle_\alpha = S - \langle a_{\alpha,\ell}^\dagger a_{\alpha,\ell} \rangle$. Converting a_α to d_μ and then to b_μ using unitary (42) and Bogolyubov (43) transformations one arrives at

$$\langle S \rangle_\alpha = S - \frac{1}{N} \sum_{\mu,\mathbf{k}} w_{\mu,\alpha}^2(\mathbf{k}) v_{\mu\mathbf{k}}^2. \quad (45)$$

Since all three sublattices are equivalent, symmetrization of (45) gives

$$\langle S \rangle = S - \frac{1}{3N} \sum_{\mu,\mathbf{k}} v_{\mu\mathbf{k}}^2, \quad (46)$$

with $v_{\mu\mathbf{k}}^2$ from (44). Calculations of the magnetization $M = \langle S \rangle/S$ and the $\langle S \rangle = 0$ Néel order boundary in the $S - \Delta$ plane are performed taking the 2D integrals in (46) numerically using (44) for the XXZ model.

Quantum suppression of the ordered moment vs anisotropy Δ is shown in Fig. 5(a) for two values of spin. Linear spin-wave theory suggests a disordered state near the Heisenberg limit for all spin values because quantum correction diverges for $\Delta \rightarrow 1$ due to vanishing energy of the flat mode. The critical value $1 - \Delta_c \approx 0.047$ for $S = 1/2$ is compared in Fig. 5(a) with the result for the DM coupling $D_{z,c} = 0.1$ (rescaling $1 - \Delta_c \Leftrightarrow \sqrt{3}D_{z,c}$), found by exact diagonalization (ED) [14,34]. Since the DM term suppresses tunneling processes within the manifold, it is reasonable to compare ED with spin-wave theory results to evaluate the accuracy of the Néel order boundary. One can see a qualitative agreement with ED and a quantitative exaggeration of the extent of the ordered phase, expected for the spin-wave approach.

Near the Heisenberg limit, one can neglect nondivergent terms in (46) and find an asymptotic expression for the Néel order boundary from $\langle S \rangle = 0 \approx S - A_1/6\omega_1$, where $A_1 = 3/4$, see (16), and $\omega_1 = \sqrt{3(1-\Delta)}/2$, see (22), leading to $1 - \Delta_c \approx 1/96S^2$, which is shown in Fig. 5(b) together with the result of the numerical integration in (46) and demonstrates an exceedingly close agreement with it.

III. NONLINEAR SPIN-WAVE THEORY

In Sec. II we have considered three anisotropic models of the kagomé-lattice antiferromagnets in the harmonic approximation and outlined the approach to taking into account other

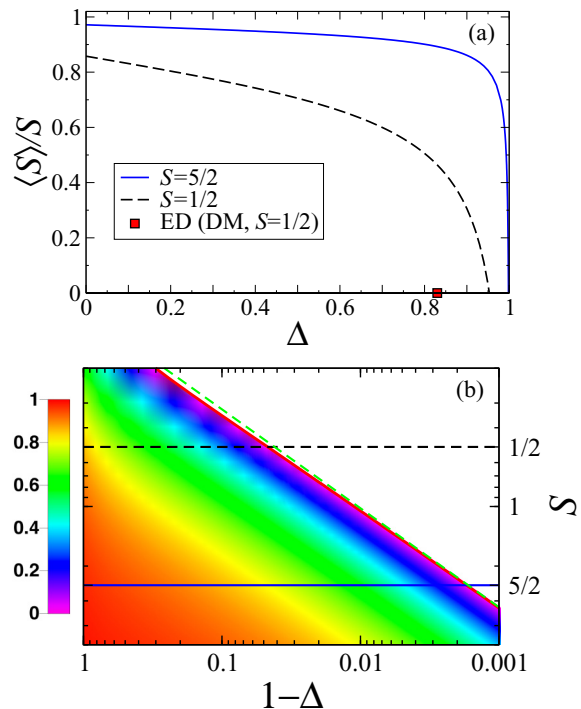


FIG. 5. (Color online) (a) Magnetization $M = \langle S \rangle/S$ vs Δ for $S = 1/2$ and $S = 5/2$. Square is the ED result for $S = 1/2$ with the DM interaction. (b) Intensity plot of the magnitude of M . Solid line is the $\langle S \rangle = 0$ Néel order phase boundary in the $S - \Delta$ plane on the log-log scale and dashed line is the asymptotic approximation for it; see text.

terms, such as further-neighbor exchanges, perturbatively. In this section, we derive the nonlinear, cubic, and quartic terms of the spin-wave $1/S$ expansion and then exemplify their role in the ground-state selection and in the spectral properties of the kagomé-lattice antiferromagnets using representative cases.

Below, we first obtain cubic and quartic terms of the spin-wave expansion to conclude the formal development of the theory. Then the cubic vertices for $\mathbf{q} = 0$ and $\sqrt{3} \times \sqrt{3}$ states allow us to proceed with calculating order-by-disorder fluctuating corrections to their ground-state energies for the XXZ and single-ion anisotropy models. Both models demonstrate a quantum phase transition between the $\mathbf{q} = 0$ and the $\sqrt{3} \times \sqrt{3}$ states as a function of anisotropy parameter. Hence both cases present rare examples of the quantum order by disorder favoring a different state from the one selected by thermal fluctuations, the latter choosing the $\sqrt{3} \times \sqrt{3}$ structure regardless of the anisotropy [2,5,7,9,10,17–19].

We then proceed with a calculation of the decay-induced effects in the structure factor $S(\mathbf{q}, \omega)$ within the DM model with J_2 . While this calculation is aimed at giving a detailed account of the spectral properties of a specific kagomé-lattice antiferromagnet described by this model, $S = 5/2$ Fe-jarosite, the outlined scenario should be applicable to a wide variety of the other flat-band frustrated spin systems [22–25]. We also note that the structure factor \mathbf{q} dependence allows one to “filter out” spectral contributions of specific modes in the portions of the \mathbf{q} space while highlighting the others, a useful phenomenon characteristic of the non-Bravais lattices.

A. Cubic terms

In the XXZ , single-ion anisotropy, and Heisenberg models, (2) with or without the anisotropies in (20) and (23), the terms that lead to the cubic anharmonic coupling of the spin waves are identical and originate from the $S_i^x S_j^z$ part of (2). These terms are also the only ones that are able to distinguish between different 120° spin configurations in these models by virtue of containing $\sin \theta_{ij} = \pm\sqrt{3}/2$ for the clockwise or counterclockwise spin rotation. In the bosonic representation they yield

$$\hat{\mathcal{H}}_3 = J\sqrt{\frac{3S}{2}} \sum_{i,j} \sin \theta_{ij} (a_i^\dagger a_j^\dagger a_j + \text{H.c.}), \quad (47)$$

where $\theta_{ij} = \theta_i - \theta_j$ is the angle between two neighboring spins as before. Clearly, the spin-wave interaction resulting from this term has different amplitude for different spin patterns. For the DM model, the DM term (27) also contributes to the cubic anharmonicity, but its structure for the $\mathbf{q} = 0$ state is identical to (47), see (32), so it gives a simple change of the overall factor in the vertex $J \rightarrow J + D_z/\sqrt{3}$.

Using (47), we now detail the derivation of the cubic vertices for the main contenders for the ground state, the $\mathbf{q} = 0$ and the $\sqrt{3} \times \sqrt{3}$ states. We begin with the $\mathbf{q} = 0$ pattern, for which $\hat{\mathcal{H}}_3$ in (47) can be rewritten as

$$\hat{\mathcal{H}}_3 = -J\sqrt{\frac{3S}{2N}} \sum_{\alpha\beta, \mathbf{k}, \mathbf{q}} \epsilon^{\alpha\beta\gamma} \cos(q\beta\alpha) a_{\alpha, \mathbf{q}}^\dagger a_{\beta, \mathbf{k}}^\dagger a_{\beta, \mathbf{p}} + \text{H.c.}, \quad (48)$$

where $\epsilon^{\alpha\beta\gamma}$ is the Levi-Civita antisymmetric tensor, $\mathbf{p} = \mathbf{k} + \mathbf{q}$, $q\beta\alpha = \mathbf{q} \cdot \boldsymbol{\rho}_{\beta\alpha}$, and $\boldsymbol{\rho}_{\beta\alpha} = \boldsymbol{\rho}_\beta - \boldsymbol{\rho}_\alpha$.

The unitary transformation (42) in (48) yields

$$\hat{\mathcal{H}}_3 = -J\sqrt{\frac{3S}{2N}} \sum_{\mathbf{k}, \mathbf{q}} \sum_{\nu\mu\eta} F_{\mathbf{q}\mathbf{k}\mathbf{p}}^{\nu\mu\eta} d_{\nu, \mathbf{q}}^\dagger d_{\mu, \mathbf{k}}^\dagger d_{\eta, \mathbf{p}} + \text{H.c.}, \quad (49)$$

where $\mathbf{p} = \mathbf{k} + \mathbf{q}$ and the amplitude is

$$F_{\mathbf{q}\mathbf{k}\mathbf{p}}^{\nu\mu\eta} = \sum_{\alpha\beta} \epsilon^{\alpha\beta\gamma} \cos(q\beta\alpha) w_{\nu, \alpha}(\mathbf{q}) w_{\mu, \beta}(\mathbf{k}) w_{\eta, \beta}(\mathbf{p}). \quad (50)$$

Finally, the Bogolyubov transformation (43) gives

$$\begin{aligned} \hat{\mathcal{H}}_3 &= \frac{1}{3!} \frac{1}{\sqrt{N}} \sum_{\mathbf{k}, \mathbf{q}} \sum_{\nu\mu\eta} V_{\mathbf{q}\mathbf{k}\mathbf{p}}^{\nu\mu\eta} b_{\nu, \mathbf{q}}^\dagger b_{\mu, \mathbf{k}}^\dagger b_{\eta, -\mathbf{p}} + \text{H.c.} \\ &+ \frac{1}{2!} \frac{1}{\sqrt{N}} \sum_{\mathbf{k}, \mathbf{q}} \sum_{\nu\mu\eta} \Phi_{\mathbf{q}\mathbf{k}\mathbf{p}}^{\nu\mu\eta} b_{\nu, \mathbf{q}}^\dagger b_{\mu, \mathbf{k}}^\dagger b_{\eta, \mathbf{p}} + \text{H.c.}, \end{aligned} \quad (51)$$

with the vertices for the ‘‘source’’ and the ‘‘decay’’ terms

$$V_{\mathbf{q}\mathbf{k}\mathbf{p}}^{\nu\mu\eta} = -J\sqrt{\frac{3S}{2}} \tilde{V}_{\mathbf{q}\mathbf{k}\mathbf{p}}^{\nu\mu\eta}, \quad \Phi_{\mathbf{q}\mathbf{k}\mathbf{p}}^{\nu\mu\eta} = -J\sqrt{\frac{3S}{2}} \tilde{\Phi}_{\mathbf{q}\mathbf{k}\mathbf{p}}^{\nu\mu\eta}, \quad (52)$$

where the symmetrized dimensionless vertices are

$$\begin{aligned} \tilde{V}_{\mathbf{q}\mathbf{k}\mathbf{p}}^{\nu\mu\eta} &= F_{\mathbf{q}\mathbf{k}\mathbf{p}}^{\nu\mu\eta} (u_{\nu\mathbf{q}} + v_{\nu\mathbf{q}})(u_{\mu\mathbf{k}} v_{\eta\mathbf{p}} + v_{\mu\mathbf{k}} u_{\eta\mathbf{p}}) \\ &+ F_{\mathbf{k}\mathbf{p}\mathbf{q}}^{\mu\eta\nu} (u_{\mu\mathbf{k}} + v_{\mu\mathbf{k}})(u_{\nu\mathbf{p}} v_{\eta\mathbf{q}} + v_{\nu\mathbf{p}} u_{\eta\mathbf{q}}) \\ &+ F_{\mathbf{p}\mathbf{q}\mathbf{k}}^{\eta\nu\mu} (u_{\eta\mathbf{p}} + v_{\eta\mathbf{p}})(u_{\nu\mathbf{q}} v_{\mu\mathbf{k}} + v_{\nu\mathbf{q}} u_{\mu\mathbf{k}}) \end{aligned} \quad (53)$$

and

$$\begin{aligned} \tilde{\Phi}_{\mathbf{q}\mathbf{k}\mathbf{p}}^{\nu\mu\eta} &= F_{\mathbf{q}\mathbf{k}\mathbf{p}}^{\nu\mu\eta} (u_{\nu\mathbf{q}} + v_{\nu\mathbf{q}})(u_{\mu\mathbf{k}} u_{\eta\mathbf{p}} + v_{\mu\mathbf{k}} v_{\eta\mathbf{p}}) \\ &+ F_{\mathbf{k}\mathbf{p}\mathbf{q}}^{\mu\eta\nu} (u_{\mu\mathbf{k}} + v_{\mu\mathbf{k}})(u_{\nu\mathbf{p}} v_{\eta\mathbf{q}} + v_{\nu\mathbf{p}} v_{\eta\mathbf{q}}) \\ &+ F_{\mathbf{p}\mathbf{q}\mathbf{k}}^{\eta\nu\mu} (u_{\eta\mathbf{p}} + v_{\eta\mathbf{p}})(u_{\nu\mathbf{q}} v_{\mu\mathbf{k}} + v_{\nu\mathbf{q}} u_{\mu\mathbf{k}}), \end{aligned} \quad (54)$$

where we have used the symmetry property $F_{\mathbf{q}\mathbf{k}\mathbf{p}}^{\nu\mu\eta} = F_{\mathbf{q}\mathbf{p}\mathbf{k}}^{\nu\mu\eta}$.

Repeating the same calculation for the $\sqrt{3} \times \sqrt{3}$ state we obtain identical expressions for the cubic spin-wave Hamiltonian and corresponding vertices, but with different amplitudes $F_{\mathbf{q}\mathbf{k}\mathbf{p}}^{\nu\mu\eta}$ expressed as

$$F_{\mathbf{q}\mathbf{k}\mathbf{p}}^{\nu\mu\eta} = i \sum_{\alpha\beta} \epsilon^{\alpha\beta\gamma} \sin(q\beta\alpha) w_{\nu, \alpha}(\mathbf{q}) w_{\mu, \beta}(\mathbf{k}) w_{\eta, \beta}(\mathbf{p}). \quad (55)$$

Explicit expressions for the unitary transformation eigenvectors $w_{\nu, \alpha}(\mathbf{q})$ of the matrix $\hat{\mathbf{A}}_{\mathbf{k}}$ and of the parameters of the Bogolyubov transformation are instrumental in deriving analytic expressions of the cubic anharmonic terms. We also note that for all models considered here, the functional form of the cubic vertices (53) and (54) is identical, with all the differences hidden in the expressions of the Bogolyubov parameters $u_{\mu\mathbf{k}}$ and $v_{\mu\mathbf{k}}$ from (44).

The role of the cubic terms in the ground-state selection and in the spectrum of the kagomé-lattice antiferromagnets is discussed below in Sec. III C and Sec. III D.

B. Quartic terms

In the Holstein-Primakoff bosonic representation of spin models, quartic terms originate from the $S_i^x S_j^x$, $S_i^y S_j^y$, and $S_i^x S_j^z$ parts of the Hamiltonian. In the models considered here, quartic terms do not help to differentiate between different states of the 120° manifold, but lead to the overall ground-state energy shift and to the Hartree-Fock corrections to the spin-wave energies. Because of the coplanar 120° spin configuration, the formal expressions for these contributions show a close similarity to the ones for the triangular-lattice Heisenberg model; see Ref. [13]. Therefore, we simply list the quartic parts of the Hamiltonians of the XXZ model and the DM term together with the expressions for the ground-state energy shift in the former model and for the spin-wave energy correction for the latter model. Technical details are offered in the Appendix.

The quartic terms in the XXZ model, (2) and (20), are

$$\begin{aligned} \hat{\mathcal{H}}_4 &= \frac{J}{2} \sum_{(ij)} \left(\frac{2\Delta + 1}{8} ((n_i + n_j) a_i a_j + \text{H.c.}) \right. \\ &\left. - \frac{2\Delta - 1}{8} (a_j^\dagger (n_i + n_j) a_i + \text{H.c.}) - n_i n_j \right), \end{aligned} \quad (56)$$

where $n_i = a_i^\dagger a_i$ and we omitted the α indices of the bosonic variables for brevity.

The quartic contribution from the DM term (27) is

$$\begin{aligned} \hat{\mathcal{H}}_{4, DM} &= \frac{D_z \sqrt{3}}{2} \sum_{(ij)} \left(\frac{1}{8} ((n_i + n_j) a_i a_j + \text{H.c.}) \right. \\ &\left. + \frac{1}{8} (a_j^\dagger (n_i + n_j) a_i + \text{H.c.}) - n_i n_j \right). \end{aligned} \quad (57)$$

By means of the Hartree-Fock decoupling [35] outlined in the Appendix, one can obtain contribution of the quartic terms to the $1/S$ series expansion of the ground-state energy of any noncollinear spin model

$$E = E_{\text{cl}} + \delta E^{(2)} + \delta E^{(3)} + \delta E^{(4)}, \quad (58)$$

where the first term is the classical energy of order $O(S^2)$, the second is the harmonic correction from \mathcal{H}_2 , $O(S)$, and the last two are from the nonlinear cubic and quartic terms, both $O(1)$. While we discuss the cubic part of this expression later, the classical and harmonic energy terms (per spin) of the series in (58) for the XXZ model are

$$E_{\text{cl}} + \delta E^{(2)} = -JS^2 - JS \left(1 - \frac{1}{3N} \sum_{\mu, \mathbf{k}} \omega_{\mu, \mathbf{k}} \right), \quad (59)$$

with the frequencies from (22). The quartic member of the series (58) for the same model is

$$\begin{aligned} \delta E_4 = -J \left[n^2 + m^2 + \bar{\Delta}^2 - (2\Delta + 1) \left(n\bar{\Delta} + \frac{m\delta}{2} \right) \right. \\ \left. + (2\Delta - 1) \left(nm + \frac{\bar{\Delta}\delta}{2} \right) \right], \quad (60) \end{aligned}$$

where the Hartree-Fock averages are introduced in a standard manner

$$n = \langle a_i^\dagger a_i \rangle, \quad m = \langle a_i^\dagger a_j \rangle, \quad \bar{\Delta} = \langle a_i a_j \rangle, \quad \delta = \langle a_i^2 \rangle, \quad (61)$$

and are given in the Appendix.

In the same order of expansion, quartic terms lead to the Hartree-Fock corrections to the linear spin-wave Hamiltonian

$$\delta \hat{\mathcal{H}}_2 = 2J \sum_{\nu, \mathbf{k}} \delta A_{\nu, \mathbf{k}} d_{\nu, \mathbf{k}}^\dagger d_{\nu, \mathbf{k}} - \frac{\delta B_{\nu, \mathbf{k}}}{2} (d_{\nu, \mathbf{k}}^\dagger d_{\nu, -\mathbf{k}}^\dagger + \text{H.c.}),$$

which yields the Hartree-Fock part of the $1/S$ contribution to the spin-wave energy

$$\varepsilon_{\nu, \mathbf{k}}^{(4)} = 2J \frac{A_{\nu, \mathbf{k}} \delta A_{\nu, \mathbf{k}} - B_{\nu, \mathbf{k}} \delta B_{\nu, \mathbf{k}}}{\omega_{\nu, \mathbf{k}}}. \quad (62)$$

Here we give expressions for $\delta A_{\nu, \mathbf{k}}$ and $\delta B_{\nu, \mathbf{k}}$ for the Heisenberg model (2) with the DM anisotropy (27) as an example,

$$\delta A_{\nu, \mathbf{k}} = \tilde{C}_1 + \frac{\tilde{C}_2 \lambda_{\nu, \mathbf{k}}}{2}, \quad \delta B_{\nu, \mathbf{k}} = -2\tilde{C}_4 - \frac{\tilde{C}_3 \lambda_{\nu, \mathbf{k}}}{2}, \quad (63)$$

where $\tilde{C}_i = C_i - d_M D_i$ and the constants are the linear combinations of the binary Hartree-Fock averages in (61) and can be found in the Appendix. We note that since the flat-mode eigenvalue $\lambda_{1, \mathbf{k}} = -1$, the quartic $1/S$ correction to its energy, $\varepsilon_{1, \mathbf{k}}^{(4)}$ in (62), is also necessarily momentum independent in all models considered here. Therefore, it is a contribution of the cubic terms which is going to introduce a fluctuation-induced dispersion in the flat mode in the same order of the $1/S$ expansion.

C. Ground-state selection

Here, we discuss the role of cubic terms (51) in the ground-state selection in the XXZ and the single-ion anisotropy models. As was mentioned above, in the case of these models, (2) with (20) and (23), classical and harmonic terms are not able to lift the degeneracy in the manifold of coplanar 120°

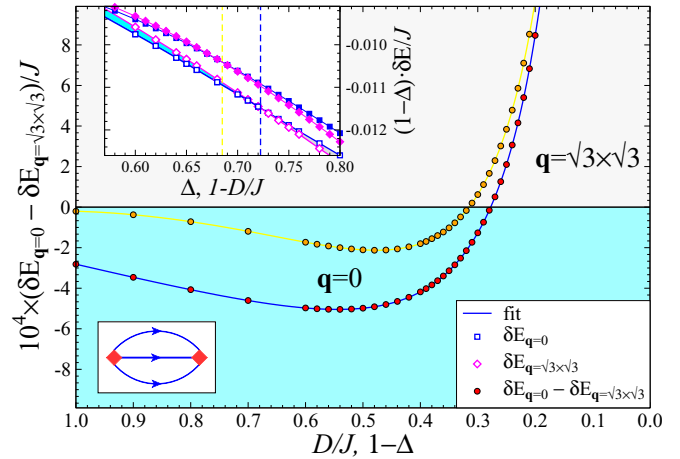


FIG. 6. (Color online) Difference of the ground-state energies of the $\mathbf{q}=0$ and $\sqrt{3} \times \sqrt{3}$ states per spin. Upper inset: energy correction $\delta E^{(3)}$ for the $\mathbf{q}=0$ (squares) and $\sqrt{3} \times \sqrt{3}$ state (diamonds). Dashed vertical lines mark the transition. Upper data points/lines in the figure and inset are for the single-ion anisotropy model, (2) with (23), and the lower are for the XXZ model, (2) with (20). Lower inset: diagram for $\delta E^{(3)}$ term (64) in the energy expansion (58).

structures. It is also easy to see from (2) that the quartic terms are also unable to differentiate between 120° states, leaving the cubic term as a sole source of the quantum order-by-disorder effect to this order in $1/S$. The same is also true for the single-ion term in (23).

The second-order energy correction from the cubic terms (51) resulting in $\delta E^{(3)}$ in (58) is represented by the diagram in the lower inset of Fig. 6 and is given by

$$\delta E^{(3)} = -\frac{1}{18N^2} \sum_{\nu\mu\eta} \sum_{\mathbf{q}, \mathbf{k}} \frac{|V_{\mathbf{q}, \mathbf{k}, -\mathbf{k}-\mathbf{q}}^{\nu\mu\eta}|^2}{\varepsilon_{\nu, \mathbf{q}} + \varepsilon_{\mu, \mathbf{k}} + \varepsilon_{\eta, -\mathbf{k}-\mathbf{q}}}, \quad (64)$$

where the energy is per spin and N is the number of unit cells. Summation over magnon branches μ, ν, η gives twenty-seven individual contributions of which ten are distinct. With the formal expression for the source vertices in (53), the energy correction in (64) is identical for the XXZ and the single-ion cases, with the differences in the expressions for the spin-wave energies $\varepsilon_{\alpha, \mathbf{k}}$ in (22) and (25) and (26), and in the $u_{\alpha\mathbf{k}}$ and $v_{\alpha\mathbf{k}}$ parameters (44) in vertices (53) for the corresponding models.

Using an explicit form for the cubic vertices for the $\mathbf{q}=0$ and $\sqrt{3} \times \sqrt{3}$ spin states, we performed a high-accuracy numerical integration in Eq. (64) and studied the quantum order-by-disorder effect. Results of these calculations are presented in Fig. 6. The quantum selection of the $\mathbf{q}=0$ state over the $\sqrt{3} \times \sqrt{3}$ counterpart for the large planar anisotropy $(1 - \Delta_c)[D_c/J] \gtrsim 0.3$ was highlighted in our previous work on the XXZ model [9]. This qualitative conclusion is in contrast with the usual behavior, in which quantum fluctuations lead to the same ground state that is selected by the thermal fluctuations. Indeed, for the classical kagomé-lattice antiferromagnets in both Heisenberg and XY limits, thermal fluctuations select the $\sqrt{3} \times \sqrt{3}$ magnetic structure as the leading instability [2,5,7,17–19] contrary to the behavior of the quantum model.

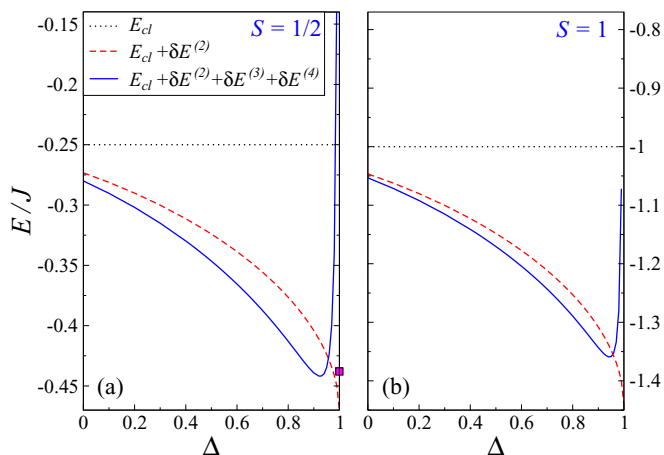


FIG. 7. (Color online) Energy per site of the $\mathbf{q}=0$ state in the XXZ model. Dotted line is for the classical term $E_{cl} = -JS^2$, dashed is $E_{cl} + \delta E^{(2)}$ in (59), and solid line is for (58) with $\delta E^{(3)}$ and $\delta E^{(4)}$ from (60) and (64). Square is the DMRG energy for the spin-liquid state [36]. (a) $S = 1/2$; (b) $S = 1$.

Here we complement the above result by the analysis of the single-ion anisotropy model (23). While the overall trend in $\delta E_{\mathbf{q}=0}^{(3)} - \delta E_{\mathbf{q}=\sqrt{3}\times\sqrt{3}}^{(3)}$ and, in particular, the transition point between the states in both models in Fig. 6 are very similar, there is a quantitative difference. As we have noted previously, the local real-space structure of the degeneracy-lifting terms is different in the XXZ and single-ion models, implying a higher-order real-space path needed for generating the ground-state selection in the latter model [27]. Figure 6 provides a strong support to this point, as the energy difference is smaller for the single-ion model by a factor 2–8 for the range of $0.3 < (1 - \Delta)[D/J] < 1$, in a qualitative agreement with the parameter of the real-space expansion being $\sim 1/z$ ($z = 4$, coordination number) [9].

We conclude the discussion of the ground state with Fig. 7, which shows the energy of the $\mathbf{q} = 0$ state in (58) vs Δ for the XXZ model for two representative spin values $S = 1/2$ and $S = 1$. Classical and harmonic contributions to the ground-state energy are also indicated by dotted and dashed lines. Note that the energy difference shown in Fig. 6 would be nearly invisible on the scale of the plot in Fig. 7. We also note that although $\delta E^{(3)}$ and $\delta E^{(4)}$ from (60) and (64) represent the entire contribution of the $O(1)$ order in the $1/S$ expansion of the ground-state energy (58), their divergences at $\Delta \rightarrow 1$ do not cancel completely, thus signifying a breakdown of the standard $1/S$ expansion at the Heisenberg limit because of the vanishing energy of the flat mode [8].

D. Spectrum and decays

We now turn to the spectral properties of the kagomé-lattice antiferromagnets. The goal of our consideration is twofold. First, we would like to highlight an unusual spectral property that has to be present in a wide variety of frustrated spin systems with excitations featuring flat branches [11]. Second, we give a detailed account of such spectral properties in a specific model that describes Fe-jarosite [20,21]. Because of that we concentrate on the out-of-plane DM-anisotropy

model, (2) with (27), of the $S = 5/2$ nearest-neighbor kagomé-lattice antiferromagnet, which closely describes Fe-jarosite in the range of small D_z . One can expect the results of this consideration to be similar to the ones for the XXZ and single-ion anisotropy models given the similarity of their harmonic spectra and anharmonic terms, even though the ground-state selection is more subtle in the later models.

1. Formalism and a qualitative discussion

Regardless of the model, using standard diagrammatic rules with the cubic terms in (51) produces the spin-wave self-energy in the form

$$\Sigma_{\mu,\mathbf{k}}(\omega) = \frac{1}{2N} \sum_{\mathbf{q},\nu\eta} \left(\frac{|\Phi_{\mathbf{q},\mathbf{k}-\mathbf{q};\mathbf{k}}^{v\eta\mu}|^2}{\omega - \varepsilon_{\nu,\mathbf{q}} - \varepsilon_{\eta,\mathbf{k}-\mathbf{q}} + i\delta} - \frac{|V_{\mathbf{q},-\mathbf{k}-\mathbf{q};\mathbf{k}}^{v\eta\mu}|^2}{\omega + \varepsilon_{\nu,\mathbf{q}} + \varepsilon_{\eta,\mathbf{k}-\mathbf{q}} - i\delta} \right), \quad (65)$$

where the first and the second terms are the decay and the source self-energies. Because of the summation over the magnon branches ν and η in the decay and source loops, there are nine terms in the sum in (65), only six of which are distinct. Note that for the DM model one has to change $J \rightarrow J + D_z/\sqrt{3}$ in the vertices.

Taken on shell, $\omega = \varepsilon_{\mu,\mathbf{k}}$, the self-energy (65) represents a strictly $1/S$ correction to the magnon energy from the cubic terms, $\Sigma_{\mu,\mathbf{k}}(\varepsilon_{\mu,\mathbf{k}}) = O(S^0)$. The other term of the same order in the $1/S$ expansion is from the quartic terms, $\varepsilon_{\nu,\mathbf{k}}^{(4)}$, which was obtained for the DM model in (62). Then, the magnon Green's function for the branch μ can be written as

$$G_{\mu}^{-1}(\mathbf{k},\omega) = \omega - \varepsilon_{\mu,\mathbf{k}} - \varepsilon_{\mu,\mathbf{k}}^{(4)} - \Sigma_{\mu,\mathbf{k}}(\omega), \quad (66)$$

which, generally, allows one to evaluate the spectral function $A_{\mu}(\mathbf{k},\omega) = -(1/\pi)\text{Im}G_{\mu}(\mathbf{k},\omega)$ of the corresponding spin-wave branch μ .

Since we are interested in the large- S limit and in the resonancelike decay phenomenon in the spectrum, the following simplification can be used. Given the off-resonance character of the source term, the frequency independence of the quartic terms, and the large- S limit of the problem, one can neglect the real part of the $1/S$ corrections to the spectrum as a first step, and approximate the self-energy in (65) by its on-shell imaginary part, i.e., $\Sigma_{\mu}(\mathbf{k},\omega) \approx i \text{Im}\Sigma_{\mu}(\mathbf{k},\varepsilon_{\mu,\mathbf{k}}) = -i\Gamma_{\mu,\mathbf{k}}$, with

$$\Gamma_{\mu,\mathbf{k}} = \frac{\pi}{2N} \sum_{\mathbf{q},\nu\eta} |\Phi_{\mathbf{q},\mathbf{k}-\mathbf{q};\mathbf{k}}^{v\eta\mu}|^2 \delta(\varepsilon_{\mu,\mathbf{k}} - \varepsilon_{\nu,\mathbf{q}} - \varepsilon_{\eta,\mathbf{k}-\mathbf{q}}), \quad (67)$$

where the summation is over magnon branches of the decay products. Using the dimensionless vertices in (54) and frequencies in (30) and (31), one can rewrite (67) as

$$\frac{\Gamma_{\mu,\mathbf{k}}}{J} = \frac{3\pi}{8N} \sum_{\mathbf{q},\nu\eta} |\tilde{\Phi}_{\mathbf{q},\mathbf{k}-\mathbf{q};\mathbf{k}}^{v\eta\mu}|^2 \delta(\omega_{\mu,\mathbf{k}} - \omega_{\nu,\mathbf{q}} - \omega_{\eta,\mathbf{k}-\mathbf{q}}), \quad (68)$$

which is explicitly independent of the spin value S . As is mentioned above, the summation over magnon branches in (68) contains six distinct terms, or potential “decay channels.” A particular decay channel may or may not be contributing to

the decays, depending on the kinematic conditions discussed below.

Before we divert our attention to a specific model, the following qualitative consideration can be made. The form in (68) suggests that $\Gamma_{\mu,\mathbf{k}} = O(J)$, which is small compared to $\varepsilon_{\mu,\mathbf{k}} = O(JS)$ in the large- S limit. Thus, generally, one can expect a regular, perturbative $1/S$ effect of broadening of the higher-energy part of the dispersive branches due to decays into the lower-energy states [12]. However, a spectacular exception to this rule must occur if both of the decay products, branches ν and η , belong to flat modes with $\omega_1 = \text{const}$. Clearly, this decay channel produces an essential singularity in $\Gamma_{\mu,\mathbf{k}}$ and $\Sigma_{\mu}(\mathbf{k},\omega)$ at the energy equal to twice the flat mode energy, the effect that can be seen as a resonancelike decay. Therefore, special care must be exercised in this case as any residual dispersion of the flat mode becomes crucial in regularizing such a singularity.

In fact, the way of removing this singularity is offered by the same $1/S$ fluctuations due to cubic terms, as the self-energy (65) also yields a dispersion for the flat mode. This can also be interpreted as fluctuation-generated further-neighbor J_2 spin-spin interactions [8,9], and such a dispersion of the flat mode has been observed in Fe-jarosite [20]. Still, this scenario implies that the fluctuation-induced flat-mode bandwidth, $W_1 \propto O(1)$, is of the order $1/S$ compared to the bandwidths of the normal dispersive modes, $W_{2(3)} \propto O(S)$.

Introducing this $1/S$ dispersion for the flat modes in (68) suggests that the near-resonance decay-induced broadening of the dispersive mode within the energy window of the width $2W_1$ near $2\omega_1$ should now scale as $\Gamma_{\mu,\mathbf{k}} = O(JS)$. This is the *same* energy scale as the spin-wave dispersion itself without any obvious additional smallness. Therefore, our analysis implies a very strong broadening, likely eliminating spectral weight nearly completely from the respective energy range even when spin S is large, providing an example of a spectacular quantum effect in an almost classical system.

Thus, in theory, as $S \rightarrow \infty$, we predict that an anomalous broadening and a wipe-out of the spectral weight should remain in the spectra of the flat-band frustrated systems, albeit in the energy window of order $O(J)$, while the spectrum width grows as $O(JS)$. In practice, we argue that such a spectacularly strong quantum effect, leading to the quasiparticle breakdown with characteristic termination points and ranges of energies dominated by broad continua, must be present in an almost classical $S = 5/2$ kagomé-lattice Fe-jarosite.

2. Decay channels in Fe-jarosite

An extensive analysis of the kinematic decay conditions in representative models of the frustrated spin systems has been provided previously [12,13]. Here, the modification of the problem is in having three different magnon branches, which modifies these condition to

$$\omega_{\mu,\mathbf{k}} = \omega_{\nu,\mathbf{q}} + \omega_{\eta,\mathbf{k}-\mathbf{q}}, \quad (69)$$

so that every decay channel $\mu \rightarrow \{\nu,\eta\}$ has to be analyzed separately. That is, for each branch μ up to six channels can be contributing independently to the decay rate

$$\Gamma_{\mu,\mathbf{k}} = \sum_{\{\nu,\eta\}} \Gamma_{\mathbf{k},\mu \rightarrow \{\nu,\eta\}}. \quad (70)$$

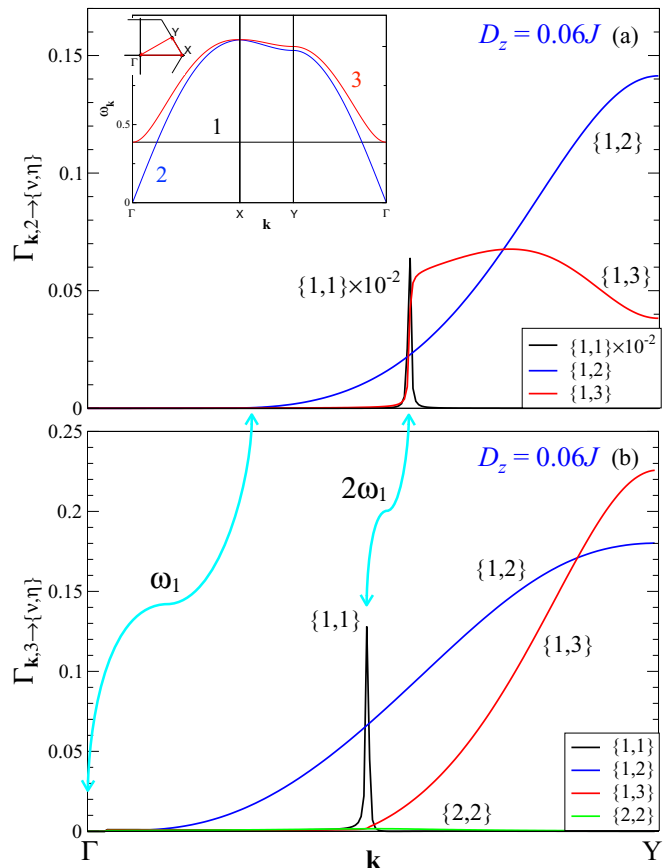


FIG. 8. (Color online) Individual contributions to the decay rate in (68) from the decay channels $\Gamma_{\mathbf{k},\mu \rightarrow \{\nu,\eta\}}$ in units of J , (a) for mode 2 and (b) for mode 3 in for the DM model. $D_z = 0.06J$, \mathbf{k} is along the ΓY direction, and artificial broadening $\delta = 0.002$ has been used. \mathbf{k} values that correspond to ω_1 and $2\omega_1$ are indicated by the arrows. Results for the “resonant” decay channel $2 \rightarrow \{1,1\}$ are scaled down by the factor 10^{-2} . Inset: harmonic frequencies $\omega_{\alpha,\mathbf{k}}$ along the representative cuts of the BZ for all three modes from Fig. 4.

While the decay conditions are model specific, Fe-jarosite offers a commonplace scenario: a predominantly nearest-neighbor Heisenberg system with subleading symmetry-breaking anisotropic term, which is responsible for lifting the flat mode to a finite energy. We, therefore, analyze the decay channels for this representative situation for a small $D_z = 0.06J$, used in fitting spin-wave spectrum of Fe-jarosite [21]. The harmonic dispersions for this value of D_z are shown in Fig. 4 and in the inset of Fig. 8(a), and we use them in our analysis.

We use the same numeration of the branches as before: 1=flat mode, 2=gapless mode (Goldstone branch), and 3=gapped dispersive mode. While the flat mode does have one active decay channel into two Goldstone modes, $1 \rightarrow \{2,2\}$, for a small range of momenta near the center of the Brillouin zone, $\mathbf{k} < \mathbf{k}_c$ where \mathbf{k}_c is the intersect point of the branches, see Fig. 8(a), its effect is truly minor and the main interest is in the decays of the dispersive modes. From the picture of harmonic energies, it is easy to see that the energy conservation in (69) can be satisfied for three (four) decay channels out of the six for the mode 2(3), one being the “resonancelike,” $2(3) \rightarrow \{1,1\}$,

mentioned above, and two (three) are “regular.” The latter are $2(3) \rightarrow \{1,2\}$ and $2(3) \rightarrow \{1,3\}$, with an additional channel for the mode $3 \rightarrow \{2,2\}$.

Using (68), we calculate contributions of the individual decay channels, $\Gamma_{\mathbf{k},\mu \rightarrow \{v,\eta\}}$, shown in Figs. 8(a) and 8(b), for modes 2 and 3 and for a representative \mathbf{k} cut of the Brillouin zone. One can see that for $2(3) \rightarrow \{1,1\}$ it gives a δ peak at $2\omega_1$, that $2(3) \rightarrow \{1,2\}$ channel has a threshold at ω_1 and $2(3) \rightarrow \{1,3\}$ at $2\omega_1$. In Fig. 8(a), the resonance decay rate is scaled down by 10^{-2} and would otherwise dwarf the rest even for the small artificial broadening of the δ function in (68).

A somewhat unexpected finding is a strong suppression of the $3 \rightarrow \{2,2\}$ and the $3 \rightarrow \{1,1\}$ channels. A closer analysis has identified different origins for them. For the $3 \rightarrow \{2,2\}$ channel, decay products involve long-wavelength excitations from the Goldstone branch, which provides an extra smallness in the decay amplitude compared with the “regular” ones. For the $3 \rightarrow \{1,1\}$ channel the situation is more subtle. One can demonstrate that the vertex $\tilde{\Phi}_{\mathbf{q},\mathbf{k}-\mathbf{q};\mathbf{k}}^{113}$ carries an extra D_z compared with the vertex for the $2 \rightarrow \{1,1\}$ channel, yielding a factor of about $1/100$ in the decay rate. The physical reason for this suppression can be hypothesized. Quasiclassically, the mode 2 is the “in-plane” mode, while modes 3 and 1 are “out of plane.” Then the in-plane mode can couple naturally to the two out-of-plane modes, while the out-of-plane mode has a hard time splitting into two.

Thus the suppression of the resonant decays of the mode 3 seems to be due to a subtle cancellation in the structure of the corresponding vertex. We note that for a realistic case of Fe-jarosite, other symmetry-breaking terms are also present, so one can expect the subtle cancellations of more symmetric models to be violated.

3. Spectrum of Fe-jarosite

We now finally approach the realistic description of the Fe-jarosite spectrum. We note that more details of this discussion is offered elsewhere [11]. As was mentioned above, the essential singularity in the dispersive modes is naturally removed by the residual dispersion of the flat mode. The experimentally observed dispersion of the flat mode [20] has been fit [21] by introducing small next-nearest neighbor exchange $J_2 = 0.03J$, ignoring its possible quantum origin. Since we do not perform a fully self-consistent calculation here, the same approach suffices for the removal of the singularity in the decay rate (68). We, thus, modify the flat-mode dispersion according to (39) and ignore other corrections from the J_2 term.

In Sec. III E we elaborate on the possible way of separating contributions of different modes in the neutron-scattering structure factor, which allows us to concentrate on individual modes. Therefore, our Fig. 9 summarizes the effects of decays on the gapless dispersive mode only, as they are most pronounced in it. We have used parameters shown in the figure with the value of $J = 3.34$ meV from the previous work [21].

The lower curve shows the on-shell $\Gamma_{2,\mathbf{k}}$ obtained from (68) with the flat-mode dispersion from (39), and it includes all three decay channels discussed above. The dashed line is the linear spin-wave energy, $\varepsilon_{2,\mathbf{k}}$, with the shaded area around it representing $\varepsilon_{2,\mathbf{k}} \pm \Gamma_{2,\mathbf{k}}$, i.e., half width at the half maximum

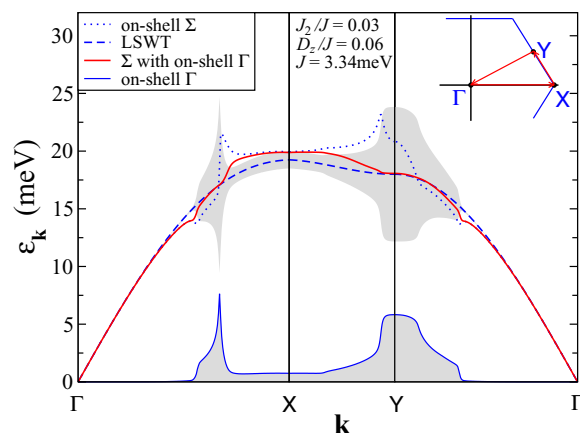


FIG. 9. (Color online) Lower curve with the shading is the on-shell $\Gamma_{2,\mathbf{k}}$ from (68). Dashed line is the linear spin-wave theory energy of the gapless dispersive mode, $\varepsilon_{2,\mathbf{k}}$, from (31). Shaded area shows the half-width boundaries of a Lorentzian peak, $\varepsilon_{2,\mathbf{k}} \pm \Gamma_{2,\mathbf{k}}$. Dotted and solid lines are different approximations for the renormalization of the real part of the self-energy in (65); see text. Parameters are as shown in the plot.

boundaries of a Lorentzian peak. We have also taken into account renormalization of the real part of the self-energy in (65), with the dotted line showing the $1/S$ on-shell result and the solid line including the effect of self-consistency by taking into account the imaginary part from $\Gamma_{2,\mathbf{k}}$ in calculation of $\text{Re}\Sigma$. One can see that the resultant effects of the nonlinear terms on the real part of the spectrum are relatively minor, in agreement with the discussion after Eq. (66).

We complement Fig. 9 by an intensity map of the spectral function, $A_2(\mathbf{k},\omega)$, for the same dispersive mode along the same representative path in the Brillouin zone and for the same parameters; see Fig. 10. Dashed and dotted lines are the spin-wave results from Fig. 9 and are guides to the eye. The magnon self-energy is approximated by its on-shell imaginary part, as discussed above. The upper cutoff of the intensity of the spectral function corresponds to the maximal height of the peaks in the nonresonant decay region in Fig. 9 and translates into the broadening $\Gamma_{\mathbf{k}} \approx 0.73$ meV for the Fe-jarosite, easily resolvable by the modern neutron-scattering experiments.

Given the large spin value, $S = 5/2$, we estimate that the ordered moment in Fe-jarosite should be nearly 90% of its classical value; see Fig. 5. It is then very natural to assume that the spectral properties should be fully describable by the harmonic spin-wave picture, the point of view taken in Ref. [21]. Indeed, our Figs. 9 and 10 demonstrate that the spin-wave excitation is sharp below the flat-band energy $\varepsilon_{1,\mathbf{k}}$ and acquires only an infinitesimal width for the energies above it. However, there is a sharp threshold at twice the bottom of the flat band minimum, $2\varepsilon_{1,\mathbf{k}}^{\min}$, above which there is a very strong broadening, reaching about one-third of the bandwidth, signifying an overdamped spectrum [11]. Above $2\varepsilon_{1,\mathbf{k}}^{\min}$ in Fig. 10 there is a broad energy band with the features that look like a rip in the spectrum, consistent with the missing spectral weight in the experimental data. This threshold singularity is also remarkably similar to the spectral signatures of the

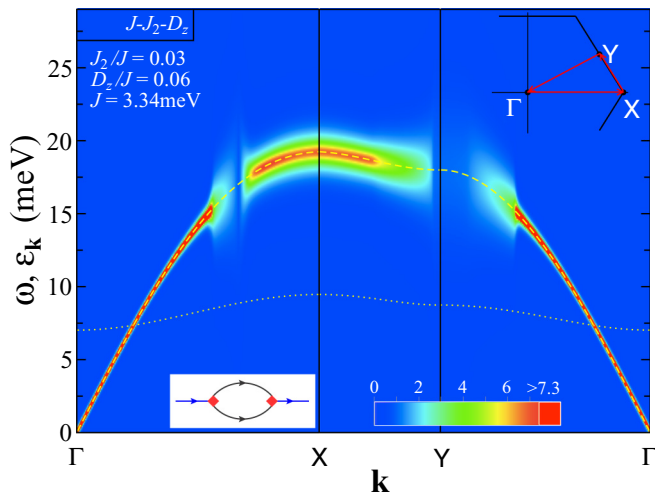


FIG. 10. (Color online) Intensity plot of the spectral function $A_2(\mathbf{k}, \omega)$ of the gapless mode in units of $(2SJ)^{-1}$ along the same path and for the same parameters as in Fig. 9 and lines are from the same figure; see text. A small broadening $\delta/2SJ = 0.002$ has been added to $\Gamma_{2,\mathbf{k}}$ in (67). Left panel inset: decay diagram.

quasiparticle breakdown phenomenon in quantum Bose liquids and $S = 1/2$ spin liquids [15,16].

Although at the energies above twice the top of the flat-band maximum, $2\varepsilon_{1,\mathbf{k}}^{\max}$, the decays are “regular,” i.e., occurring due to other, nonresonant channels, they are still providing a measurable broadening to the spectrum, so it is instructive to compare the two regions. The regular decays result in the maximal values of Γ of order $0.2\text{--}0.3J$, an agreement with the similar effects in triangular-lattice antiferromagnets [13] and other frustrated spin systems [12]. The maximal broadening in the resonant-decay region is $\Gamma \approx 1.7J$ for the Fe-jarosite model, which is larger than the effect of the regular decays by a factor close to 5 ($= 2S$). This is in remarkably close accord with the qualitative argument on the scaling of the resonance decay rate with the spin value, provided after Eq. (68) above.

While a more detailed description of the spectral features of Fe-jarosite is given elsewhere [11], we would like to highlight here a different, perhaps more dramatic view on the drastic transformations in its spectrum in the range of energies that falls within the resonant-decay band. In Fig. 11 we show an intensity plot of the constant-energy cut of the spectral function, $A_2(\mathbf{k}, \omega)$, of the same dispersive mode as in Figs. 9 and 10 for the energy 18 meV, which is close to the middle of the resonant-decay region. The dashed lines show the expectations from the linear spin-wave theory of where the contours of sharp, well-defined peaks should have occurred. Instead, one can observe strong deviation from such expectations, characterized by a broadening, massive redistribution of the spectral weight into different regions of \mathbf{k} space, together with the multitude of intriguing features, which are related to the van Hove singularities in the two-particle density of states of the flat-band decay products [13]. Altogether, Figs. 9, 10, and 11 offer a convincing evidence of the highly nontrivial and very strong quantum effects

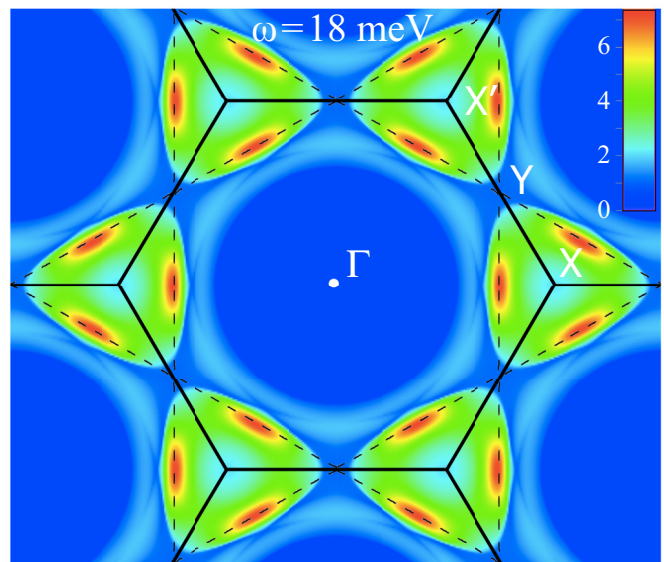


FIG. 11. (Color online) Intensity map of $A_2(\mathbf{k}, \omega)$ in units of $(2SJ)^{-1}$ vs \mathbf{k} throughout the Brillouin zone for the same set of parameters as in Fig. 9 for $\omega = 18$ meV. The upper cutoff of the intensity scale corresponds to the broadening $\Gamma_{2,\mathbf{k}}$ of 0.73 meV for the Fe-jarosite values of S and J . Dashed black lines are peak positions from the linear spin-wave theory.

in the dynamical response of a nearly classical flat-band kagomé-lattice antiferromagnet, which are facilitated by the nonlinear couplings.

E. Dynamical structure factor

Inelastic neutron scattering cross section is directly related to the diagonal components of the dynamical structure factor, or the spin-spin dynamical correlation function, given by

$$S^{i_0 i_0}(\mathbf{q}, \omega) = \int_{-\infty}^{\infty} \frac{dt}{2\pi} e^{i\omega t} \langle S_{\mathbf{q}}^{i_0}(t) S_{-\mathbf{q}}^{i_0} \rangle, \quad (71)$$

where i_0 refers to the laboratory frame $\{x_0, y_0, z_0\}$ and

$$S_{\mathbf{q}}^{i_0} = \sum_{\alpha} S_{\alpha, \mathbf{q}}^{i_0} \quad (72)$$

involves summation over the spins α in the unit cell.

Because of the coplanar spin configuration in the considered kagomé-lattice antiferromagnets, transformation from the laboratory reference frame of i_0 to the local spin basis of (2) yields a mix of different diagonal and off-diagonal terms in the structure factor [37], which conveniently separate into the in-plane and out-of-plane parts of $S^{\text{tot}}(\mathbf{q}, \omega)$. Assuming equal contribution of all three i_0 components to the neutron-scattering cross section [37] and using the mapping of spins on bosons (6) allows one to perform a straightforward $1/S$ ranking of different contributions to the structure factor, in which the transverse components, as usual, dominate the longitudinal and mixed terms.

The subsequent algebra involves the two-step transformation (42) and (43) from the Holstein-Primakoff bosons to the quasiparticles, yielding the leading contributions to the structure factor as directly related to the spin-wave spectral

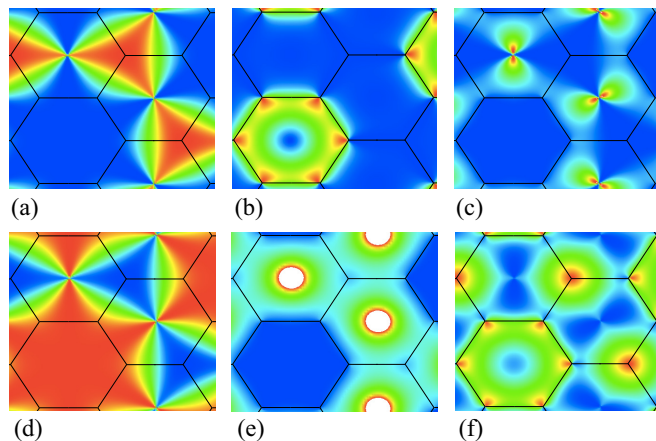


FIG. 12. (Color online) Kinematic form factors: $F_{v\mathbf{q}}^{\text{out}}$ for the (a) flat, (b) dispersive gapless, and (c) dispersive gapped mode; $F_{v\mathbf{q}}^{\text{in}}$ for the (d) flat, (e) dispersive gapless, and (f) dispersive gapped mode. $F_{2\mathbf{q}}^{\text{in}}$ in (e) diverges at some Γ points as $\omega_{2,\mathbf{q}}^{-1}$.

functions $A_\nu(\mathbf{q}, \omega)$

$$\mathcal{S}^{\text{in(out)}}(\mathbf{q}, \omega) \approx \sum_\nu F_{\nu\mathbf{q}}^{\text{in(out)}} A_\nu(\mathbf{q}, \omega), \quad (73)$$

where we introduced kinematic form factors

$$\begin{aligned} F_{\nu\mathbf{q}}^{\text{in}} &= \frac{S}{2}(u_{\nu\mathbf{q}} + v_{\nu\mathbf{q}})^2(1 - R_{\nu\mathbf{q}}), \\ F_{\nu\mathbf{q}}^{\text{out}} &= \frac{S}{2}(u_{\nu\mathbf{q}} - v_{\nu\mathbf{q}})^2(1 + 2R_{\nu\mathbf{q}}), \end{aligned} \quad (74)$$

with

$$R_{\nu\mathbf{q}} = \frac{1}{2} \sum_{\alpha \neq \alpha'} w_{\nu,\alpha}(\mathbf{q}) w_{\nu,\alpha'}(\mathbf{q}). \quad (75)$$

An important property of the kinematic form factors in (74) is their \mathbf{q} dependence. They are modulated in the \mathbf{q} space and are typically suppressed in one of the Brillouin zones while being maximal in the others. This effect is characteristic to the neutron scattering in the non-Bravais lattices and is, in a way, similar to the effect known as the Bragg peak extinction for the elastic scattering in such lattices. Because of that property, one may be able to focus on a specific excitation branch without intermixing contributions from the others by selecting a particular component of the structure factor in a particular Brillouin zone.

Our Fig. 12 shows $F_{\nu\mathbf{q}}^{\text{in(out)}}$ for three branches of excitations in the Fe-jarosite model. It demonstrates that such a “filtering out” can be quite useful. For example, the out-of-plane component of the structure factor, $\mathcal{S}^{\text{out}}(\mathbf{q}, \omega)$, should be dominated in one of the three distinct Brillouin zones by the spectral function $A_2(\mathbf{q}, \omega)$ of only one of the dispersive modes. This feature can be utilized in the neutron-scattering experiments.

Lastly, we highlight another quantitative way of analyzing $\mathcal{S}(\mathbf{q}, \omega)$. Assuming that one can focus on a particular excitation branch as mentioned above, one can suggest that a faithful representation of the inverse lifetime (linewidth) $\Gamma_{\mu\mathbf{q}}$ from (67) and its distribution in \mathbf{q} space across the Brillouin zone can be obtained from the moments of the dynamical structure

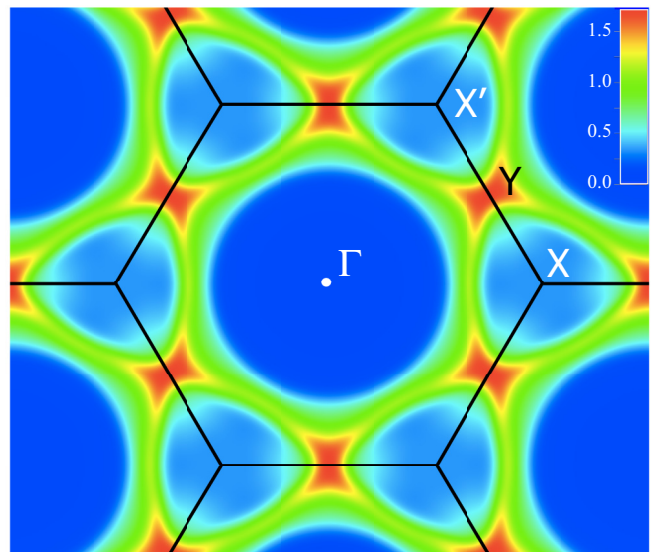


FIG. 13. (Color online) 2D map of the inverse lifetime from (76) in units of J in the \mathbf{q} space. A small artificial Gaussian \mathbf{q} broadening with $\sigma = 0.02\pi/a$ was used to mimic instrumental resolution. The scale is given in the inset and the maximal value of $\Gamma_{2,\mathbf{q}}^{\text{max}} \approx 1.7J$ corresponds to about 6 meV for Fe-jarosite.

factor as [38]

$$\tilde{\Gamma}_{\mathbf{q}} = \sqrt{\langle \omega^2 \mathcal{S}(\mathbf{q}, \omega) \rangle - \langle \omega \mathcal{S}(\mathbf{q}, \omega) \rangle^2}, \quad (76)$$

where $\langle \omega^n \mathcal{S}(\mathbf{q}, \omega) \rangle = \int \omega^n \mathcal{S}(\mathbf{q}, \omega) d\omega$ are the moments of the structure factor and normalization $\langle \mathcal{S}(\mathbf{q}, \omega) \rangle = 1$ is assumed. Then, this experimentally unbiased procedure would allow extracting a 2D \mathbf{q} map of the quasiparticle broadening. We demonstrate the effectiveness of this approach in Fig. 13, which shows an example of such a map derived using the procedure in (76) from a *Gaussian* form $A_2(\mathbf{q}, \omega)$, i.e., the Gaussian function with a maximum at $\varepsilon_{2,\mathbf{q}}$ and the width $\Gamma_{2,\mathbf{q}}$. As expected, the extracted map of $\tilde{\Gamma}_{\mathbf{q}}$ is nearly identical to the map of $\Gamma_{2,\mathbf{q}}$ itself. However, for a more natural Lorentzian form of $A_2(\mathbf{q}, \omega)$ one can show that the extracted map corresponds to $\tilde{\Gamma}_{\mathbf{q}} \propto \sqrt{\omega_{\text{max}} \Gamma_{2,\mathbf{q}}}$, where ω_{max} is the upper limit of the integration over ω in the moments in (76). Importantly, this result is still providing direct information on the quasiparticle broadening map, albeit on a different scale. Therefore, aside from demonstrating at which momenta the decays are most intense, the suggested procedure also provides another way of “fingerprinting” of the broadening due to resonancelike decay into the flat modes.

IV. CONCLUSIONS

In summary, we have provided a systematic consideration of the nonlinear $1/S$ expansion of several anisotropic models of the kagomé-lattice antiferromagnets. We have demonstrated the role of the nonlinear terms in the quantum order-by-disorder selection of the ground state and presented strong evidence of the rare case of quantum and thermal fluctuations favoring different ground states in two of these models. We have provided a detailed analysis of the excitation spectrum of the $S = 5/2$ iron-jarosite to illustrate

our proposed general scenario of drastic transformations in the spectra of the flat-band frustrated magnets. Our study calls for further neutron-scattering experiments in these systems.

ACKNOWLEDGMENTS

We acknowledge useful discussions with Collin Broholm, Christian Batista, Federico Becca, Andrey Chubukov, Andreas Läuchli, Young Lee, Kittiwit Matan, George Jackeli, Steven White, and Zhenyue Zhu. This work was supported by the U.S. Department of Energy, Office of Science, Basic Energy Sciences under Grant No. DE-FG02-04ER46174. A.L.C. would like to thank Aspen Center for Physics and the Kavli Institute for Theoretical Physics where different stages of this work were advanced. The work at Aspen was supported by NSF Grant No. PHYS-1066293 and the research at KITP was supported by NSF Grant No. NSF PHY11-25915.

APPENDIX: HARTREE-FOCK CORRECTIONS

The quartic terms in (56) yield a correction to the ground-state energy given by the four-boson averages, which are decoupled into the products of the binary Hartree-Fock averages (61) using Wick's theorem

$$\begin{aligned} \langle a_i^\dagger a_i a_j^\dagger a_j \rangle &= n^2 + m^2 + \bar{\Delta}^2, \\ \langle a_i^\dagger a_i a_i a_j \rangle &= 2n\bar{\Delta} + m\delta, \\ \langle a_j^\dagger a_j a_i a_i \rangle &= 2nm + \bar{\Delta}\delta, \end{aligned} \quad (\text{A1})$$

where the Hartree-Fock averages are obtained similar to the calculation of the staggered magnetic moment in (45). Namely, for the on-site averages $n = \langle a_{\alpha,\ell}^\dagger a_{\alpha,\ell} \rangle$ and $\delta = \langle a_{\alpha,\ell} a_{\alpha,\ell} \rangle$, following the transformations (42) and (43) from a_α to d_μ and to b_μ and using equivalence of all three sublattices one

arrives at the symmetrized expressions

$$\begin{aligned} n &= \langle a_{\alpha,\ell}^\dagger a_{\alpha,\ell} \rangle = \frac{1}{3N} \sum_{\mu,\mathbf{k}} v_{\mu\mathbf{k}}^2, \\ \delta &= \langle a_{\alpha,\ell} a_{\alpha,\ell} \rangle = \frac{1}{3N} \sum_{\mu,\mathbf{k}} u_{\mu\mathbf{k}} v_{\mu\mathbf{k}}, \end{aligned} \quad (\text{A2})$$

with $u_{\mu\mathbf{k}}$ and $v_{\mu\mathbf{k}}$ from (44). For the nearest-neighbor two-site averages, the same transformations lead to

$$\begin{aligned} m &= \langle a_{\alpha,\ell}^\dagger a_{\beta,\ell'} \rangle = \frac{1}{N} \sum_{\mu,\mathbf{k}} f_{\beta\alpha}(\mathbf{k}) v_{\mu\mathbf{k}}^2, \\ \bar{\Delta} &= \langle a_{\alpha,\ell} a_{\beta,\ell'} \rangle = \frac{1}{N} \sum_{\mu,\mathbf{k}} f_{\beta\alpha}(\mathbf{k}) u_{\mu\mathbf{k}} v_{\mu\mathbf{k}}, \end{aligned} \quad (\text{A3})$$

where $f_{\beta\alpha}(\mathbf{k}) = \cos(k_{\beta\alpha}) w_{\mu,\alpha}(\mathbf{k}) w_{\mu,\beta}(\mathbf{k})$, $\alpha \neq \beta$, $w_{\mu,\alpha}(\mathbf{k})$ are the components of the eigenvector in the transformation (42), and $k_{\beta\alpha} = \mathbf{k} \cdot \boldsymbol{\rho}_{\beta\alpha}$ with $\boldsymbol{\rho}_{\beta\alpha} = \boldsymbol{\rho}_\beta - \boldsymbol{\rho}_\alpha$ as before. Although it seems that the two-site averages may depend on the choice of α and β , one can verify that all three possible combinations of $\alpha \neq \beta$ pairs yield the same answer.

Quartic terms also yield Hartree-Fock contributions to the linear spin-wave dispersions via (62). The corresponding constants for the Heisenberg and DM terms in (63) are

$$\begin{aligned} C_1 &= -n + \frac{3\bar{\Delta}}{2} - \frac{m}{2}, & C_2 &= -m + \frac{3\delta}{4} - \frac{n}{2}, \\ C_3 &= -\bar{\Delta} + \frac{3n}{2} - \frac{\delta}{4}, & C_4 &= \frac{3m}{8} - \frac{\bar{\Delta}}{8}, \\ D_1 &= n - \frac{\bar{\Delta}}{2} - \frac{m}{2}, & D_2 &= m - \frac{\delta}{4} - \frac{n}{2}, \\ D_3 &= \bar{\Delta} - \frac{n}{2} - \frac{\delta}{4}, & D_4 &= -\frac{m}{8} - \frac{\bar{\Delta}}{8}. \end{aligned} \quad (\text{A4})$$

-
- [1] J. T. Chalker, P. C. W. Holdsworth, and E. F. Shender, *Phys. Rev. Lett.* **68**, 855 (1992).
[2] D. A. Huse and A. D. Rutenberg, *Phys. Rev. B* **45**, 7536(R) (1992).
[3] M. E. Zhitomirsky, *Phys. Rev. Lett.* **88**, 057204 (2002).
[4] S. Capponi, O. Derzhko, A. Honecker, A. M. Läuchli, and J. Richter, *Phys. Rev. B* **88**, 144416 (2013).
[5] A. B. Harris, C. Kallin, and A. J. Berlinsky, *Phys. Rev. B* **45**, 2899 (1992).
[6] M. Taillefermier, J. Robert, C. L. Henley, R. Moessner, and B. Canals, *Phys. Rev. B* **90**, 064419 (2014).
[7] J. N. Reimers and A. J. Berlinsky, *Phys. Rev. B* **48**, 9539 (1993).
[8] A. Chubukov, *Phys. Rev. Lett.* **69**, 832 (1992); *J. Appl. Phys.* **73**, 5639 (1993).
[9] A. L. Chernyshev and M. E. Zhitomirsky, *Phys. Rev. Lett.* **113**, 237202 (2014).
[10] O. Götze and J. Richter, *Phys. Rev. B* **91**, 104402 (2015).
[11] A. L. Chernyshev, *Phys. Rev. B* **92**, 094409 (2015).
[12] M. E. Zhitomirsky and A. L. Chernyshev, *Rev. Mod. Phys.* **85**, 219 (2013).
[13] A. L. Chernyshev and M. E. Zhitomirsky, *Phys. Rev. B* **79**, 144416 (2009).
[14] O. Cépas, C. M. Fong, P. W. Leung, and C. Lhuillier, *Phys. Rev. B* **78**, 140405 (2008).
[15] M. B. Stone, I. A. Zaliznyak, T. Hong, C. L. Broholm, and D. H. Reich, *Nature (London)* **440**, 187 (2006).
[16] T. Masuda, A. Zheludev, H. Manaka, L.-P. Regnault, J.-H. Chung, and Y. Qiu, *Phys. Rev. Lett.* **96**, 047210 (2006).
[17] C. L. Henley, *Phys. Rev. B* **80**, 180401(R) (2009).
[18] S. E. Korshunov, *Phys. Rev. B* **65**, 054416 (2002).
[19] M. S. Rzchowski, *Phys. Rev. B* **55**, 11745 (1997).
[20] K. Matan, D. Grohol, D. G. Nocera, T. Yildirim, A. B. Harris, S. H. Lee, S. E. Nagler, and Y. S. Lee, *Phys. Rev. Lett.* **96**, 247201 (2006).
[21] T. Yildirim and A. B. Harris, *Phys. Rev. B* **73**, 214446 (2006).
[22] N. d' Ambrumenil, O. A. Petrenko, H. Mutka, and P. P. Deen, *Phys. Rev. Lett.* **114**, 227203 (2015).
[23] C. Wu, D. Bergman, L. Balents, and S. Das Sarma, *Phys. Rev. Lett.* **99**, 070401 (2007).
[24] G. Jackeli and A. Avella, [arXiv:1504.01435](https://arxiv.org/abs/1504.01435).

- [25] K. Matan, Y. Nambu, Y. Zhao, T. J. Sato, Y. Fukumoto, T. Ono, H. Tanaka, C. Broholm, A. Podlesnyak, and G. Ehlers, *Phys. Rev. B* **89**, 024414 (2014).
- [26] R. J. Baxter, *J. Math. Phys.* **11**, 784 (1970).
- [27] M. E. Zhitomirsky (unpublished).
- [28] A. Zorko, S. Nellutla, J. van Tol, L. C. Brunel, F. Bert, F. Duc, J.-C. Trombe, M. A. de Vries, A. Harrison, and P. Mendels, *Phys. Rev. Lett.* **101**, 026405 (2008).
- [29] H. Yoshida, Y. Michiue, E. Takayama-Muromachi, and M. Isobe, *J. Mater. Chem.* **22**, 18793 (2012).
- [30] I. Rousochatzakis, J. Richter, R. Zinke, and A. A. Tsirlin, *Phys. Rev. B* **91**, 024416 (2015).
- [31] M. Elhajal, B. Canals, and C. Lacroix, *Phys. Rev. B* **66**, 014422 (2002).
- [32] Y. Huh, L. Fritz, and S. Sachdev, *Phys. Rev. B* **81**, 144432 (2010).
- [33] J. von Delft and C. L. Henley, *Phys. Rev. B* **48**, 965 (1993).
- [34] L. Messio, O. Cépas, and C. Lhuillier, *Phys. Rev. B* **81**, 064428 (2010).
- [35] T. Oguchi, *Phys. Rev.* **117**, 117 (1960).
- [36] S. Yan, D. A. Huse, and S. R. White, *Science* **332**, 1173 (2011).
- [37] M. Mourigal, W. T. Fuhrman, A. L. Chernyshev, and M. E. Zhitomirsky, *Phys. Rev. B* **88**, 094407 (2013).
- [38] We are thankful to Collin Broholm for this suggestion.